Journal of
Mechanics of
Materials and Structures

LARGE-AMPLITUDE DYNAMIC ANALYSIS OF STIFFENED PLATES WITH FREE EDGES

Anirban Mitra, Prasanta Sahoo and Kashinath Saha

Volume 6, No. 6 July–August 2011

mathematical sciences publishers

JOURNAL OF MECHANICS OF MATERIALS AND STRUCTURES
Vol. 6, No. 6, 2011

LARGE-AMPLITUDE DYNAMIC ANALYSIS OF STIFFENED PLATES WITH FREE EDGES

ANIRBAN MITRA, PRASANTA SAHOO AND KASHINATH SAHA

Large-amplitude free-vibration analysis of stiffened plates subjected to uniformly distributed transverse loading with free flexural boundary conditions is presented. The free edge is taken with different combinations of clamped and simply supported end conditions for three types of stiffened plates classified according to number and orientation of stiffeners. The computational domain is divided into an adequate number of subdomains based on the number, orientation, and location of stiffeners to generate the appropriate grid of computation points. Nonlinear strain displacement relations are considered in the formulation but the effects of shear deformation have been neglected. The analysis involves two steps. First the static displacement field of the system is solved for. The second step takes up the free-vibration analysis on the basis of the known static displacement field. The mathematical formulation of the static problem is based on the principle of minimum potential energy, whereas Hamilton's principle has been applied for the dynamic analysis. The results are validated with the published results of other researchers. The dynamic behavior is presented in the form of backbone curves in a dimensionless frequency-amplitude plane. Three-dimensional mode shape plots are also presented along with contour plots in a few specific cases.

A list of symbols can be found on page 911.

1. Introduction

In marine construction and aerospace structures stiffened plates are extensively used due to their enhanced stiffness and stability characteristics. They also have widespread application in many branches of modern civil, mechanical, and structural engineering. Hence, investigation of the dynamic behavior of stiffened plates has always been an area of immense interest to researchers. Research work on the dynamic characteristics of stiffened plates has a long history as different researchers have employed different methodologies to perform dynamic analysis of such structures. The comprehensive review [Mukherjee and Mukhopadhyay 1986] documents different numerical and analytical tools used in earlier years to study the dynamic behavior of stiffened plates.

Aksu and Ali [1976] developed a variational technique in conjunction with finite difference formulation to obtain natural frequencies and mode shapes of eccentrically stiffened rectangular plates having a single stiffener. Their formulation considered in-plane displacements and inertia in the direction of the stiffener and the total energy of the system was minimized with respect to discretized displacement components. This free-vibration analysis was later extended to cross-stiffened plates thus taking into account

The first author acknowledges the research support received from AICTE, India, vide File No.: 1-10/RID/NDF/PG/(17)2008-09 Dated: 13.03.2009.

Keywords: stiffened plate, geometric nonlinearity, large-amplitude vibration, variational methods, backbone curves.

in-plane inertia effects for two directions in [Aksu 1982]. In [Prathap and Varadan 1978] large-amplitude, free flexural vibrations of simply supported and clamped thin elastic orthotropic stiffened plates with immovable and movable in-plane edges were studied. The governing dynamic equations were derived in terms of nondimensional parameters and solved on the basis of a single-term vibration mode shape by making use of Galerkin's method. Varadan and Pandalai [1979] obtained modal equations for nonlinear free vibration of eccentrically stiffened elastic rectangular plates through Lagrange's equation and an approximate analytical solution based on one-term transverse displacement was determined. They analyzed plates having clamped boundary conditions with movable in-plane edges and observed hardening-type nonlinearity.

Mukherjee and Mukhopadhyay [1988] performed free-vibration analysis of eccentrically stiffened plates using an isoparametric quadratic stiffened plate bending element. They included the effect of shear deformation in the formulation and studied the effects of eccentricity, shape, and torsional stiffness on the natural frequencies and mode shapes of the system. In [Koko and Olson 1992] free-vibration analysis of rectangular plates with discrete stiffeners was carried out utilizing the superelements and including the effects of bending and in-plane effects as well as beam torsion and lateral bending motion. In [Rao et al. 1993b] a large-amplitude free flexural vibration study of eccentrically stiffened plates incorporating in-plane and shear deformation effects was presented. Harik and Guo [1993] introduced a compound finite element model based on small deflection and thin plate theory to examine eccentrically stiffened plates in free vibration. Their formulation considered membrane forces for the plate and axial forces in the stiffener. In [Chen et al. 1994] a spline compound strip method was proposed, where the plate was discretized in only one direction, for analyzing the free-vibration problem of stiffened plates. Bedair and Troitsky [1997] analyzed eccentrically and concentrically stiffened simply supported plates on the basis of energy formulation and mathematical programming techniques and studied the effect of variation in plate and stiffener geometric parameters on the fundamental frequency of the system.

Although substantial research has been carried out in the field of vibrations of stiffened plates, interest in this field has not diminished. Vibration analysis of stiffened plates using hierarchical finite elements with a set of local trigonometric interpolation functions was presented in [Barrette et al. 2000]. In [Zeng and Bert 2001] a differential quadrature analysis of the free vibration of eccentrically stiffened plates having simply supported or clamped boundaries at all edges was implemented. In [Peng et al. 2006] free vibration and stability analysis of stiffened plates via the first-order shear deformable theory and mesh-free Galerkin method was performed. Sapountzakis and Mokos [2008] developed an improved model and obtained eigenfrequencies as a general solution for dynamic analysis of plates stiffened by arbitrarily positioned parallel beams. In [Dozio and Ricciardi 2009] a computationally efficient combined analytical-numerical method was presented for low-frequency free-vibration analysis of thin rectangular plates stiffened by a small number of light stiffeners.

A general method taking into account the nonuniform torsional response of the stiffener for free vibration of plates and shells stiffened by beams of arbitrary cross-section was introduced in [Vörös 2009]. In [Xu et al. 2010] an analytical method was put forward for the vibration analysis of plates stiffened by any number of beams of arbitrary lengths and placement angles considering coupling at an interface of plate and beam. In [Deb Nath et al. 2010] an analytical solution of elastic fields for a stiffened plate subjected to axial tension and pure bending was obtained using an alternative displacement potential approach.

The majority of the dynamic studies are confined to stiffened plates with simply supported or clamped boundaries; only in few cases are a combination of simply supported and clamped-end conditions considered. Works on stiffened plates having free boundaries are also limited. In [Bapu Rao et al. 1978] an experimental study was carried out to determine the resonant frequencies and mode shapes of rib-stiffened skew cantilever plates by holographic interferometry. In [Irie et al. 1982] a stiffened trapezoidal cantilever plate with a clamped end and three free boundaries was analyzed and the natural frequencies and mode shapes were numerically calculated. However, some works considering unstiffened plates with free edges are available in literature. In [Rossi et al. 1998] small-amplitude transverse vibration of a rectangular orthotropic plate with a free edge and a concentrated mass was considered. In [Shuyu 2001] an analytical method was presented to predict the natural frequency of flexural vibration of rectangular thin plates with free boundary conditions. In [Wang and Xu 2010] discrete singular convolution was utilized to determine nondimensional frequency parameters for clamped (CCCC), clamped with one free edge (CFCC), and free (FFFF) rectangular plates.

A review of the existing literature reveals that studies are primarily focused on free-vibration analysis of stiffened plates with simply supported, clamped, and a combination of both boundary conditions, whereas studies on stiffened plates with free edges are limited. It is also noted that the emphasis is mainly on developing different methodologies to obtain the natural frequencies compared to studying the variations in the dynamic behavior corresponding to changes in system geometry and boundary conditions. Works on large-amplitude dynamic behavior, specifically the effect of loaded vibration amplitude on the natural frequency of stiffened plates, are also rare. We investigate large-amplitude dynamic behavior of stiffened plates for various boundary conditions including a single free edge. It also looks into the effect of vibration amplitude on loaded natural frequency. The results for large-amplitude behavior are presented in terms of backbone curves in the dimensionless amplitude-frequency plane. These results have been documented for the first six vibration modes of stiffened plates under uniformly distributed transverse loading. Vibration mode shapes are also provided corresponding to the minimum and maximum amplitudes of vibration. Unlike in finite element analysis (FEA), where the physical domain is discretized into smaller finite elements, the present semianalytical formulation is associated with the whole domain, that is, the assumed displacement field is a function of the whole physical domain. As a result, the number of algebraic equations to be solved is substantially reduced compared to FEA.

2. Mathematical formulation

A thin rectangular plate ($a \times b \times t_p$) orthogonally stiffened by eccentric stiffeners parallel to the edges of the plate is shown in Figure 1, which also depicts the significant dimensions of the system and the coordinate system for the present analysis. It is assumed that the stiffeners are rigidly attached to the plate such that no relative motion can take place and no field discontinuity can occur between the two. Although the figure shows only one stiffener along each of the coordinate directions, the mathematical formulation is carried out for multiple stiffeners having generalized location in both directions. The number of stiffeners in the x and y-directions are represented by ns_x and ns_y, respectively, and the location of the q-th stiffener along the y-direction and the p-th stiffener along the x-direction are denoted by x^q_{stf} and y^p_{stf}. The eccentricity (e^p_x, e^q_y) of the stiffeners is quantified by the perpendicular distance between the centroid (CG) of the stiffener cross-section and the midplane of the plate. Only rectangular stiffener

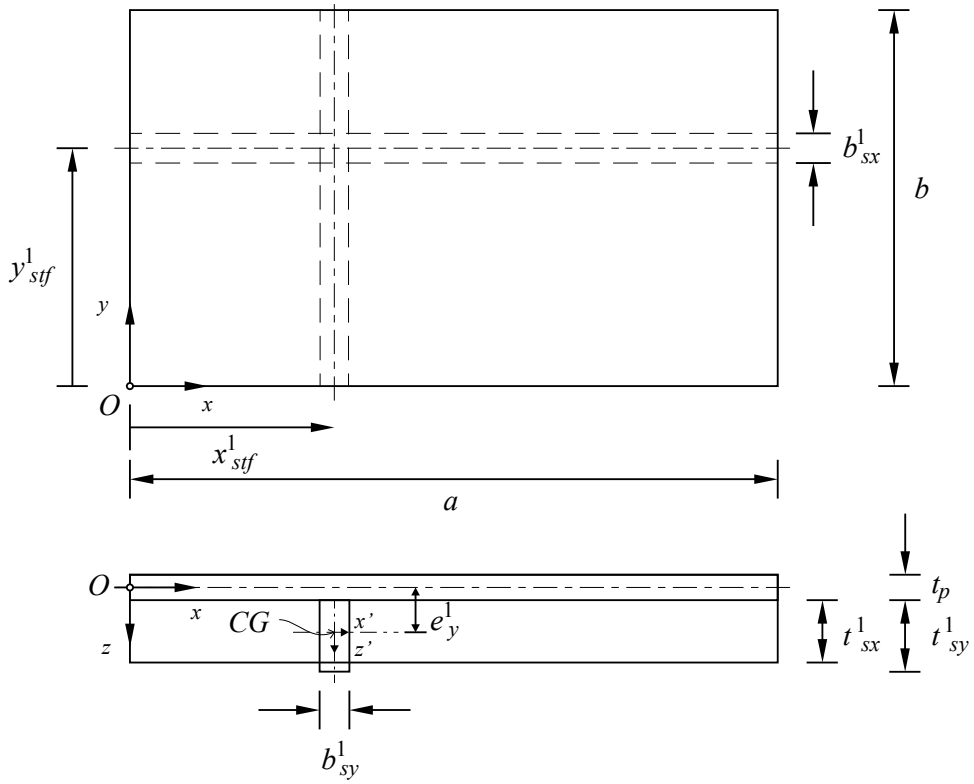

Figure 1. Stiffened plate with significant dimensions and coordinate system.

cross-sections are considered: $(b^p_{sx} \times t^p_{sx})$ for the p-th stiffener parallel to the x-axis and $(b^q_{sy} \times t^q_{sy})$ for the q-th stiffener along the y-axis. The mathematical formulation is further based on the assumptions that the plate and stiffener materials are isotropic, homogeneous, and linearly elastic and the plate thickness (t_p) is small enough compared to its lateral dimensions (a and b) so that the effects of shear deformation and rotary inertia can be ignored.

The physical domain in the x-y coordinate system as shown in Figure 1 is converted to the computational domain by normalizing the midplane coordinates as $\xi = x/a$ and $\eta = y/b$. In this ξ-η computational plane, Gauss points are generated along the two orthogonal coordinate directions and constant ξ and constant η lines are drawn through the generated Gauss points. Intersections of these constant ξ and constant η lines provide a grid of reference points for computations. However, a stiffener can be placed at any location inside the domain and as the locations of the Gauss points are fixed, there may not be a sufficient number of computation points around a stiffener. Hence, depending on the number, orientation, and location of the stiffeners the domain is decomposed into subdomains, which have their own Gauss points spaced in the same ratio as the original domain. This technique helps to have an adequate number of computation points around the location of stiffeners and boundaries of the plate so that the displacement field can be captured accurately. Such decomposed domains with modified grids corresponding to different types of plates having different stiffener orientations and positions are shown in Figure 2.

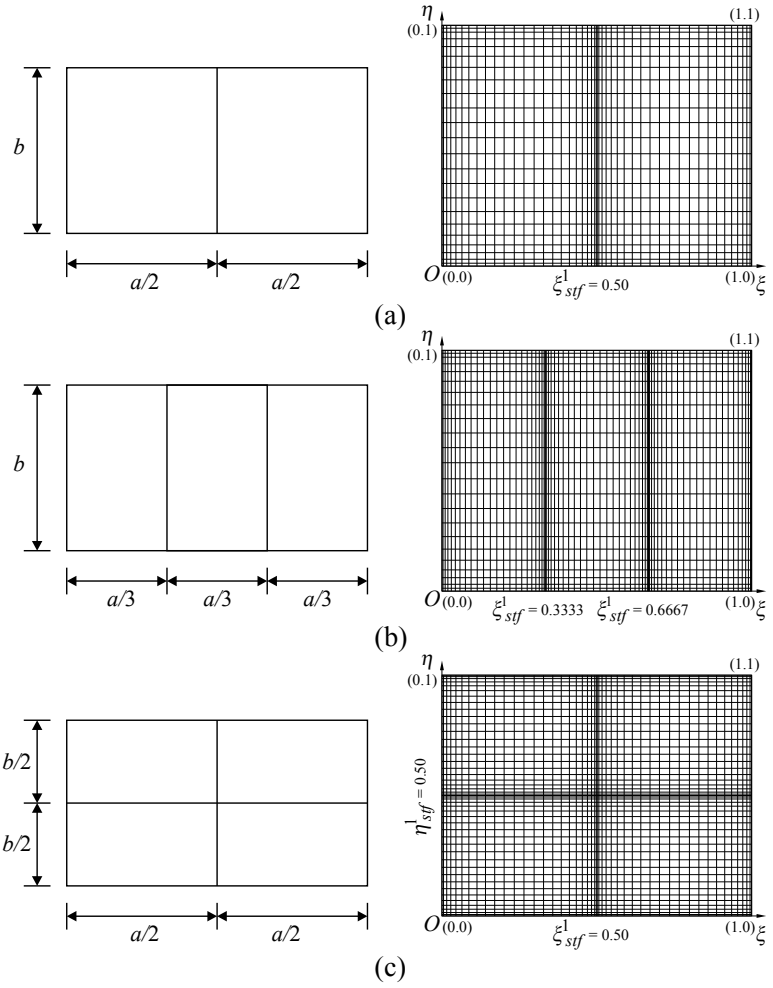

Figure 2. Decomposed computational domain along with schematic representations for (a) uniaxially single stiffened (UASS), (b) uniaxially double stiffened (UADS), and (c) biaxially cross stiffened (BACS) plates.

In nonlinear vibration, frequency is a function of the vibration amplitude and the nature of the deflected profile [Bikri et al. 2003; Das et al. 2009]; moreover, the amplitude of vibration at a point within a vibrating continuous system depends on the location. In studying the effect of vibration amplitude on the dynamic behavior of stiffened plates, the maximum amplitude of vibration is taken as representative of the amplitude. The deflection profile of a system is dependent on the boundary conditions of the system and the nature of loading to which it is subjected. Different boundary conditions may arise from the different combinations of clamped, simply supported, and free end conditions of a plate. However, the present paper only deals with combinations of simply supported and clamped boundary conditions with a single free edge, under transverse uniformly distributed loading (UDL).

Large-amplitude free-vibration analysis of a nonlinear system is essentially the same as free-vibration analysis of the system subjected to a static load producing such large-amplitude deflection [Crandall

1956]. Here, the system is assumed to execute small-amplitude vibration about the statically deflected equilibrium configuration as opposed to large-amplitude vibration about its undeformed equilibrium position. Hence, the present large-amplitude free-vibration analysis of stiffened plates is performed in two steps. First, large displacement is statically imposed by applying uniform transverse loading on the stiffened plate and then the free-vibration analysis is performed as an eigenvalue problem to identify the loaded natural frequency. The static analysis yields the initial deflection profile, which is used in the subsequent free-vibration analysis. As the dynamic problem is solved on the basis of the solution of the static displacement field, the effect of a statically imposed large amplitude of vibration is incorporated into the dynamic system. The mathematical formulation for both the static and dynamic problems is based on the variational form of the energy principle. Nonlinear strain displacement relations are considered in order to incorporate geometric nonlinearity in the system.

2.1. ***Static analysis.*** The principle of minimum potential energy [Reddy 2002] can be mathematically expressed as

$$\delta(U+V)=0. \tag{1}$$

Here, V is the work function or potential of the external forces and U is the total strain energy stored in the system. For a stiffened plate under an externally applied uniformly distributed load of intensity p, the total potential energy is given by

$$V=-(ab)\int_0^1\int_0^1 (pw)\,d\xi\,d\eta. \tag{2}$$

The total strain energy (U) of the system consists of two components, namely the strain energy of the plate (U_p) and the total strain energy stored in all the stiffeners (U_s). In the case of large-displacement analysis of plates, both bending and stretching effects are taken into consideration. So, the strain energy of the plate (U_p) also consists of two parts: strain energy due to pure bending (U_b) and strain energy due to stretching (U_m) of its midplane. The expressions of U_b and U_m are well-known for rectangular plates [Saha et al. 2004] and are indicated here for ready reference:

$$\begin{aligned}
U_b &= \frac{D}{2}(ab)\int_0^1\int_0^1\left[\left\{\frac{1}{a^2}(w_{,\xi\xi})+\frac{1}{b^2}(w_{,\eta\eta})\right\}^2+2(1-\nu)\frac{1}{a^2b^2}\{(w_{,\xi\eta})^2-(w_{,\xi\xi})(w_{,\eta\eta})\}\right]d\xi\,d\eta,\\
U_m &= \frac{E_pt_p}{2(1-\nu^2)}(ab)\int_0^1\int_0^1\left[\frac{1}{a^2}(u_{,\xi})^2+\frac{1}{a^3}(u_{,\xi})(w_{,\xi})^2+\frac{1}{b^2}(v_{,\eta})^2+\frac{1}{b^3}(v_{,\eta})(w_{,\eta})^2\right.\\
&\quad+\frac{1}{4}\left\{\frac{1}{a^2}(w_{,\xi})^2+\frac{1}{b^2}(w_{,\eta})^2\right\}^2+2\nu\left\{\frac{1}{ab}(u_{,\xi})(v_{,\eta})+\frac{1}{2a^2b}(v_{,\eta})(w_{,\xi})^2+\frac{1}{2ab^2}(u_{,\xi})(w_{,\eta})^2\right\}\\
&\quad\left.+\frac{1-\nu}{2}\left\{\frac{1}{b^2}(u_{,\eta})^2+\frac{2}{ab}(u_{,\eta})(v_{,\xi})+\frac{1}{a^2}(v_{,\xi})^2+\frac{2}{ab^2}(u_{,\eta})(w_{,\xi})(w_{,\eta})+\frac{2}{a^2b}(v_{,\xi})(w_{,\xi})(w_{,\eta})\right\}\right]d\xi\,d\eta,
\end{aligned} \tag{3}$$

where E_p, ν, and D ($=E_pt_p^3/12(1-\nu^2)$) are the elastic modulus, Poisson's ratio, and the flexural rigidity of the plate, respectively. The displacement fields of the plate along the x, y, and z-directions are represented by u, v, and w, respectively. The expression for strain energy stored in the stiffeners (U_s) can be written as $U_s=\sum_{p=1}^{ns_x}U_{sx}^p+\sum_{q=1}^{ns_y}U_{sy}^q$, where U_{sx}^p and U_{sy}^q are strain energies stored in the p-th stiffener along the x-direction and the q-th stiffener along the y-direction, respectively. In order to derive the expressions for strain energies of the individual stiffeners a compatible strain distribution at the line

joining the plate and the stiffener is assumed. Hence, the axial strain of a stiffener along the x-direction is derived from the expression $\varepsilon^p_{sx} = \varepsilon_{px}|_{z=t_p/2} - (z - t_p/2)w_{,xx} - y_s v_{,xx}$, where the plate strain at $z = t_p/2$ is denoted by $\varepsilon_{px}|_{z=t_p/2}$ and y_s denotes the distance from the local minor axis. Substituting for the plate strain, $\varepsilon_{px}|_{z=t_p/2} = u_{,x} + 0.5(w_{,x})^2 - (t_p/2)w_{,xx}$, the expression for the total strain of an x-direction stiffener is obtained as $\varepsilon^p_{sx} = u_{,x} + 0.5(w_{,x})^2 - zw_{,xx} - y_s v_{,xx}$. So, the axial strain of a stiffener along the x-direction includes axial strain due to bending action about the major axis, stretching of the neutral axis, and bending action about the minor axis. It should be pointed out that the effect of shear deformation due to direct shear and torsion has not been taken into consideration while calculating the total axial strain. Substituting the total strain in the generalized expression of strain energy, $U^p_{sx} = (E_s/2)\int_{\text{vol}} (\varepsilon^p_{sx})^2 dV$, the final expression of the strain energy stored in a x-direction stiffener is obtained. Similarly, the strain energy expression of a y-direction stiffener can be obtained and the final expression of total stiffener strain energy (U_s) is given by

$$
\begin{aligned}
U_s = \sum_{p=1}^{ns_x} \frac{E_s a}{2} \int_0^1 \Bigg[& \frac{(I^p_y + A^p_y e^{p2}_x)}{a^4}(w_{,\xi\xi})^2 + \frac{(I^p_{yz} + A^p_y (b\eta^p_{\text{stf}})^2)}{a^4}(v_{,\xi\xi})^2 \\
& - Q^p_y \left\{ \frac{2}{a^3}(u_{,\xi})(w_{,\xi\xi}) + \frac{1}{a^4}(w_{,\xi\xi})(w_{,\xi})^2 \right\} + A^p_y \left\{ \frac{1}{a^2}(u_{,\xi})^2 + \frac{1}{4a^4}(w_{,\xi})^4 + \frac{1}{a^3}(u_{,\xi})(w_{,\xi})^2 \right\} \Bigg] d\xi \\
& + \sum_{q=1}^{ns_y} \frac{E_s b}{2} \int_0^1 \Bigg[\frac{(I^q_x + A^q_x e^{q2}_y)}{b^4}(w_{,\eta\eta})^2 + \frac{(I^q_{xz} + A^q_x (a\xi^q_{\text{stf}})^2)}{b^4}(u_{,\eta\eta})^2 - Q^q_x \left\{ \frac{2}{b^3}(v_{,\eta})(w_{,\eta\eta}) \right. \\
& \left. + \frac{1}{b^4}(w_{,\eta\eta})(w_{,\eta})^2 \right\} + A^q_x \left\{ \frac{1}{b^2}(v_{,\eta})^2 + \frac{1}{4b^4}(w_{,\eta})^4 + \frac{1}{b_3}(v_{,\eta})(w_{,\eta})^2 \right\} \Bigg] d\eta. \quad (4)
\end{aligned}
$$

Here, E_s is the elastic modulus of the stiffener material. I^q_x ($= b^q_{sy} {t^q_{sy}}^3/12$), I^p_y ($= b^p_{sx} {t^p_{sx}}^3/12$) and I^q_{xz} ($= {b^q_{sy}}^3 t^q_{sy}/12$), I^p_{yz} ($= {b^p_{sx}}^3 t^p_{sx}/12$) are moments of inertia about the major and minor axes of the stiffener cross-section. Q^p_y ($= A^q_x e^q_y$), Q^q_x ($= A^p_y e^p_x$) are the first moment of area about the plate midplane and A^p_y, A^q_x are the cross-sectional areas of the p-th x and q-th y-direction stiffeners, respectively. In the expressions of the energy functionals ξ and η are the dimensionless forms of the midplane coordinates which are associated with the computational domain.

2.1.1. *Approximate displacement fields.* The plate displacement fields (w, u, and v) can be approximately expressed as linear combinations of unknown coefficients d_i as:

$$
w(\xi,\eta) = \sum_{i=1}^{nw} d_i \phi_i(\xi,\eta), \quad u(\xi,\eta) = \sum_{i=nw+1}^{nw+nu} d_i \alpha_{i-nw}(\xi,\eta), \quad v(\xi,\eta) = \sum_{i=nw+nu+1}^{nw+nu+nv} d_i \beta_{i-nw-nu}(\xi,\eta), \quad (5)
$$

where $\phi(\xi,\eta)$, $\alpha(\xi,\eta)$, and $\beta(\xi,\eta)$ are sets of orthogonal functions for w, u, and v, respectively. The functions $\phi_i(\xi,\eta)$ are associated with displacements due to bending, whereas $\alpha_i(\xi,\eta)$ and $\beta_i(\xi,\eta)$ describe stretching of the midplane of the plate. Appropriate start functions for these orthogonal sets are selected in such a way that they satisfy the flexural and membrane boundary conditions of the plate. The two-dimensional (2D) start functions are generated from one-dimensional (1D) functions corresponding to the two coordinate directions. The 1D starting functions for transverse displacement are taken to be the beam deflection functions, derived from the static deflection shape of the beam under uniform loading,

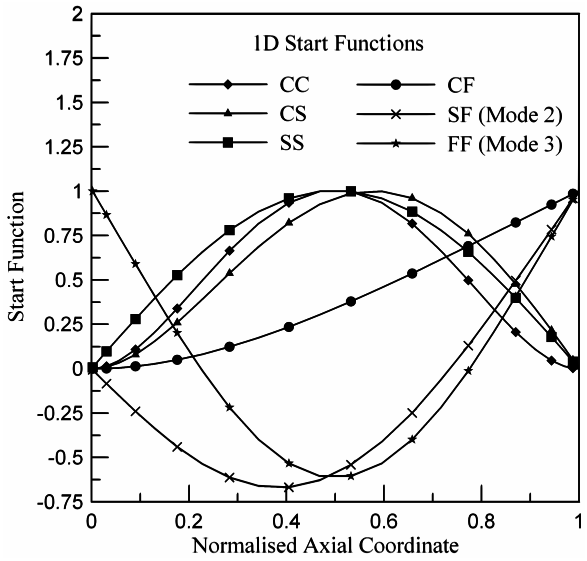

Figure 3. Plots of 1D beam functions.

corresponding to the boundary condition of the plate along the particular coordinate axis. A complete set with 21 different boundary conditions may arise from the different combinations of clamped (C), simply supported (S), and free (F) end conditions of a plate. But it is found that six basic beam functions, represented as CC, CS, CF, SS, SF, and FF, are sufficient to generate 2D start functions corresponding to all the classical boundary conditions possible for a plate. Both transcendental and polynomial functions are used to describe these 1D beam functions [Blevins 1981] and they are graphed in Figure 3.

As per the requirements of the numerical scheme, all the functions are described numerically within the computational domain at the selected Gauss points. The higher-order 1D functions are generated through a numerical implementation of the Gram–Schmidt orthogonalization procedure. However, the necessary rigid body modes for SF and FF beams are incorporated by inserting appropriate functions into the corresponding sets of orthogonal functions. The 2D functions are obtained through ordered multiplication of the 1D functions for two orthogonal directions and are specified for various boundary conditions involving a single free edge in Table 1. The notation for the boundary conditions of the plate has been specified through its edge conditions, starting from the edge $x = 0$ and proceeding counterclockwise.

Boundary condition	Start function for $w(\phi_1(\xi, \eta))$
CCCF	$\xi^2(1-\xi)^2\big(\cosh(A\eta) - \cos(A\eta) + B\{\sinh(A\eta) - \sin(A\eta)\}\big)$
CCSF	$\xi^2(3-5\xi+2\xi^2)\big(\cosh(A\eta) - \cos(A\eta) + B\{\sinh(A\eta) - \sin(A\eta)\}\big)$
CSCF	$\xi^2(1-\xi)^2\big(\cosh(C(1-\eta)) - \cos(C(1-\eta)) + D\{\sinh(C(1-\eta)) - \sin(C(1-\eta))\}\big)$
CSSF	$\xi^2(3-5\xi+2\xi^2)\big(\cosh(C(1-\eta)) - \cos(C(1-\eta)) + D\{\sinh(C(1-\eta)) - \sin(C(1-\eta))\}\big)$
SCSF	$\sin(\pi\xi)\big(\cosh(A\eta) - \cos(A\eta) + B\{\sinh(A\eta) - \sin(A\eta)\}\big)$
SSSF	$\sin(\pi\xi)\big(\cosh(C(1-\eta)) - \cos(C(1-\eta)) + D\{\sinh(C(1-\eta)) - \sin(C(1-\eta))\}\big)$

Table 1. Start functions for assumed displacement fields w.

The start functions for stretching displacement of the plate (u and v) come from in-plane or membrane boundary conditions and zero displacement is assumed at the edges ($u=0$ at $\xi=0$, 1 and $v=0$ at $\eta=0$, 1) to obtain the 1D starting polynomial functions. It should be pointed out that at the free end of the plate the transverse displacements are unrestricted, but the in-plane boundary condition is immovable, that is, displacements are restricted at all the ends including the free edge. Similar to the previous case, the 2D base functions are generated by multiplying the 1D start functions for the two orthogonal directions; these functions are given by $\alpha_1(\xi,\eta)=\{\xi(1-\xi)\}.\{\eta(1-\eta)\}$ and $\beta_1(\xi,\eta)=\{\xi(1-\xi)\}.\{\eta(1-\eta)\}$. However, in this case the higher-order functions are generated from the start functions following a two-dimensional implementation of the Gram–Schmidt orthogonalization scheme. The Gram–Schmidt orthogonalization principle and its two-dimensional implementation have been discussed in detail in [Saha et al. 2004; Das et al. 2009]. It should be noted that the generated functions are for the total domain and they need to be broken down in terms of the subdomains. These sets of functions for the subdomains are derived by carrying out interpolation operations on the total functions and are represented by ϕ_i^{mn}, α_i^{mn}, β_i^{mn}, where $m=1,\ldots,ns_y+1$ and $n=1,\ldots,ns_x+1$.

2.1.2. *Governing system of equations.* Substituting the complete energy expressions and the approximate displacement fields into (1), the set of system governing equations in matrix form is obtained as

$$[K(\{d\})]\{d\}=\{f\}. \tag{6}$$

Here, $[K]$, $\{d\}$, and $\{f\}$ are stiffness matrix, vector of unknown coefficients, and load vector, respectively. The total stiffness matrix $[K]$ of the system is given by $[K]=[K_b]+[K_m]+\sum_{p=1}^{ns_x}[K_{sx}]^p+\sum_{q=1}^{ns_y}[K_{sy}]^q$, where $[K_b]$ and $[K_m]$ are contributions from the bending and stretching action of the plate, and $[K_{sx}]^p$ and $[K_{sy}]^q$ represent the stiffness matrices of the p-th stiffener along the x-direction and the q-th stiffener along the y-direction, respectively. The details of the elements of the stiffness matrices and load vector are furnished in the Appendix.

2.1.3. *Solution methodology for static displacement field.* As large displacement induced by geometric nonlinearity is taken into consideration, the stiffness matrix $[K]$ includes elements that contain the unknown coefficients $\{d\}$, to be determined subsequently. The stiffness matrices for the stiffeners also include some terms containing the unknown coefficients. As a result the system of governing equations presented in (6) becomes nonlinear in nature and cannot be solved directly. Hence, the solution methodology specially adopted to solve the set of nonlinear equations employs an iterative procedure utilizing a direct substitution technique with a successive relaxation scheme [Cook et al. 1989]. At the start of the solution procedure necessary parameters that cater to the iterative scheme, for example, the relaxation parameter (λ), error limit (ε), etc., are chosen along with a starting load value. The linear component of the stiffness matrix $[K_b]$ is computed and an initial guess (generally taken as 0) for the unknown coefficients is assumed. The total stiffness matrix $[K]$ is calculated on the basis of the assumed values and a new set of unknown coefficients is determined from the expression $\{d\}^{(n+1)}=[K(\{d\}^{(n)})]^{-1}\{f\}$, where n denotes the iteration counter. A comparison between the calculated values and the corresponding values in the previous iteration is carried out to determine the error. If the error comes out to be within the predefined limit of tolerance, convergence is achieved. Otherwise, if the error is outside the specified value the next iteration is performed with modified values of the unknown coefficients, computed by the relation $\{d\}=\{d\}_{\text{old}}+\lambda(\{d\}-\{d\}_{\text{old}})$. Once convergence is achieved for a particular load step, an

increment is provided to the load and the present solution is taken as the initial guess for the next load step.

2.2. ***Dynamic analysis.*** The governing set of equations for the dynamic analysis is derived following Hamilton's principle, which is expressed as

$$\delta\left(\int_{\tau_1}^{\tau_2}(T-U)\,d\tau\right)=0. \tag{7}$$

According to Hamilton's principle a dynamic system can be characterized by two energy functionals, kinetic energy and potential energy. In the case of a free vibration analysis the potential energy is made up of only the strain energy of the system, as the potential of the external forces is reduced to zero. So, in the mathematical expression T and U represent the total kinetic energy of the system and the total strain energy stored in the system. The variational operator and time coordinate are denoted by δ and τ, respectively. The total kinetic energy (T) is a summation of the plate kinetic energy (T_p) and stiffener kinetic energy (T_s), that is,

$$T=T_p+T_s, \qquad \text{where } T_s=\sum_{p=1}^{ns_x}T_{sx}^{p}+\sum_{q=1}^{ns_y}T_{sy}^{q}. \tag{8}$$

T_{sx}^{p} and T_{sy}^{q} are kinetic energies of the p-th stiffener along the x-direction and the q-th stiffener along the y-direction, respectively. The expressions for the kinetic energies of plate and individual stiffeners are, in terms of dynamic displacement fields,

$$\begin{aligned}
T_p &= \tfrac{1}{2}\rho_p t_p(ab)\int_0^1\int_0^1(\dot{w}^2+\dot{u}^2+\dot{v}^2)\,d\xi\,d\eta,\\
T_{sx}^{p} &= \tfrac{1}{2}\rho_s t_{sx}^{p}(ab_{sx}^{p})\int_0^1(\dot{w}^2+\dot{u}^2+\dot{v}^2)\,d\xi,\\
T_{sy}^{q} &= \tfrac{1}{2}\rho_s t_{sy}^{q}(bb_{sy}^{q})\int_0^1(\dot{w}^2+\dot{u}^2+\dot{v}^2)\,d\eta,
\end{aligned} \tag{9}$$

where ρ_p and ρ_s are the densities of the plate and stiffener materials. The expressions of strain energies for the plate (U_b and U_m) and stiffeners (U_s) are identical to those given by (3) and (4). These energy functionals are determined from the assumed transverse ($w(\xi,\eta,\tau)$) and in-plane ($u(\xi,\eta,\tau)$ and $v(\xi,\eta,\tau)$) dynamic displacement fields, which are associated with the midplane of the plate. The assumed dynamic displacements are separable in space and time and can be approximately represented by finite linear combinations of orthogonal admissible functions and a new set of unknown coefficients, denoted by $\{c\}$:

$$\begin{aligned}
w(\xi,\eta,\tau) &= \sum_{i=1}^{nw}c_i\phi_i e^{i\omega\tau},\\
u(\xi,\eta,\tau) &= \sum_{i=nw+1}^{nw+nu}c_i\alpha_{i-nw}e^{(i-nw)\omega\tau},\\
v(\xi,\eta,\tau) &= \sum_{i=nw+nu+1}^{nw+nu+nv}c_i\beta_{i-nw-nu}e^{(i-nw-nu)\omega\tau}.
\end{aligned} \tag{10}$$

In these expressions ω is the natural frequency of the system and $\{c\}$ denotes the eigenvectors in matrix form which represent the contribution of the individual space functions in a particular vibration frequency mode. The spatial functions $\phi_i(\xi,\eta)$, $\alpha_i(\xi,\eta)$, and $\beta_i(\xi,\eta)$ are identical to those for the static analysis in (5). Substitution of the kinetic (T) and strain energy (U) expressions along with the dynamic displacement fields gives the governing equation of the dynamic system in the following form:

$$-\omega^2[M]\{c\}+[K]\{c\}=0, \tag{11}$$

where $[K]$ is the stiffness matrix of the system at the deflected configuration. This implies that the unknown parameters obtained from the converged static solution are used to compute the starting values for solving the dynamic problem. In the above expression, $[M]$ is the mass matrix that includes contributions from the plate ($[M_p]$) and the x and y-direction stiffeners ($[M_{sx}]$ and $[M_{sy}]$). So, the final expression for the total mass matrix is obtained as $[M]=[M_p]+[M_{sx}]+[M_{sy}]$. The form of $[M]$ is given by

$$[M]=\begin{bmatrix} M_{11} & 0 & 0 \\ 0 & M_{22} & 0 \\ 0 & 0 & M_{33} \end{bmatrix},$$

where

$$[M_{11}]=\rho_p t_p(ab)\sum_{j=1}^{nw}\sum_{i=0}^{nw}\int_0^1\int_0^1\phi_i\phi_j\,d\xi\,d\eta+\sum_{p=1}^{ns_x}\left[\rho_s t_{sx}^p(ab_{sx}^p)\sum_{j=1}^{nw}\sum_{i=1}^{nw}\int_0^1\phi_i\phi_j\,d\xi\right]+\sum_{q=1}^{ns_y}\left[\rho_s t_{sy}^q(bb_{sy}^q)\sum_{j=1}^{nw}\sum_{i=1}^{nw}\int_0^1\phi_i\phi_j\,d\eta\right],$$

$$[M_{22}]=\rho_p t_p(ab)\sum_{j=nw+1}^{nw+nu}\sum_{i=nw+1}^{nw+nu}\int_0^1\int_0^1\alpha_{i-nw}\alpha_{j-nw}\,d\xi\,d\eta+\sum_{p=1}^{ns_x}\left[\rho_s t_{sx}^p(ab_{sx}^p)\sum_{j=nw+1}^{nw+nu}\sum_{i=nw+1}^{nw+nu}\int_0^1\alpha_{i-nw}\alpha_{j-nw}\,d\xi\right]+\sum_{q=1}^{ns_y}\left[\rho_s t_{sy}^q(bb_{sy}^q)\sum_{j=nw+1}^{nw+nu}\sum_{i=nw+1}^{nw+nu}\int_0^1\alpha_{i-nw}\alpha_{j-nw}\,d\eta\right],$$

$$[M_{33}]=\rho_p t_p(ab)\sum_{j=nw+nu+1}^{nw+nu+nv}\sum_{i=nw+nu+1}^{nw+nu+nv}\int_0^1\int_0^1\beta_{i-nw-nu}\beta_{j-nw-nu}\,d\xi\,d\eta+\sum_{p=1}^{ns_x}\left[\rho_s t_{sx}^p(ab_{sx}^p)\sum_{j=nw+nu+1}^{nw+nu+nv}\sum_{i=nw+nu+1}^{nw+nu+nv}\int_0^1\beta_{i-nw-nu}\beta_{j-nw-nu}\,d\xi\right]+\sum_{q=1}^{ns_y}\left[\rho_s t_{sy}^q(bb_{sy}^q)\sum_{j=nw+nu+1}^{nw+nu+nv}\sum_{i=nw+nu+1}^{nw+nu+nv}\int_0^1\beta_{i-nw-nu}\beta_{j-nw-nu}\,d\eta\right].$$

The governing equation of the dynamical system (11) can be alternatively written as

$$[[M]^{-1}[K]]\{c\}=\omega^2\{c\}.$$

This is a standard eigenvalue problem which is solved numerically through IMSL routines. The square roots of the computed eigenvalues give the free vibration frequencies at the statically deflected configuration of the stiffened plate and are called the loaded natural frequencies. The amplitude of free vibration is obtained from the transverse displacement fields associated with the eigenvalues. The plot of the loaded natural frequencies against the corresponding amplitudes in a nondimensional plane represents the backbone curve of the system. The eigenvectors corresponding to the eigenvalues are utilized to determine the mode shapes of the vibrating system.

3. Results and discussion

Our analysis is carried out for three different types of stiffened plates — uniaxially single stiffened, uniaxially double stiffened, and biaxially cross stiffened — under a uniformly distributed load. The classification is according to the number and orientation of the stiffeners, as shown schematically in Figure 2, which also presents the decomposed computational domains that provide an improved grid corresponding to the three different types of stiffened plates. As stated earlier, for each of the three types of plates, six classical flexural boundary conditions are considered: CCCF, CCSF, CSCF, CSSF, SCSF, and SSSF, each letter indicating an edge condition, moving counterclockwise beginning with the edge $x = 0$. Thus there is a single free edge, always at $y = b$, and the other edges are variously clamped or simply supported. These flexural boundary conditions dictate the choice of start functions for the definition of transverse deflection (w). The base functions for the in-plane displacement (u and v) of the plate are derived from the membrane boundary conditions, which are modeled as immovable edges in all cases.

The process of generation of start functions for both transverse and deformation displacement has been discussed in Section 2.1.1, and Table 1 presents base functions for individual cases of flexural end conditions. The Gram–Schmidt orthogonalization principle is utilized to generate a complete set of higher-order functions and adequate measures are taken to insert rigid body modes wherever necessary. The number of functions for each of the plate displacements (u, v, and w) is taken as 25 (5×5), where the numbers in the parentheses indicate the number of functions corresponding to the two orthogonal directions. Due to the general nature of the formulation any other classical flexural boundary conditions can be handled through this method. It should also be mentioned that the present methodology can be applied for any other transverse loading pattern, mathematically expressible in terms of the coordinates.

The analysis is based on determining the static displacement field first and subsequently computing the eigenvalues of the corresponding dynamic problem based on the known static displacement field. The solution methodology of the static problem involves an iterative numerical scheme using successive relaxation due to presence of nonlinearity in the stiffness matrix. The tolerance value of the error limit (ε) for the numerical iterative scheme is fixed at 0.50% and the relaxation parameter (λ) is taken as 0.50. The solution of the dynamic problem is obtained using IMSL routines.

To determine the number of Gauss points to be used for generation of results a convergence study is carried out on a uniaxially single stiffened plate under uniformly distributed transverse loading. The details of the plate and stiffener geometry, material properties, and boundary conditions are provided in the figure's legend. For a transverse load of 100 kPa intensity, the normalized maximum deflection ($w_{\max}/t_p$) of the system is plotted against a number of Gauss points (ng) in Figure 4. A choice of 24 Gauss points for the present work is made from the convergence study. The initial choice of number of Gauss

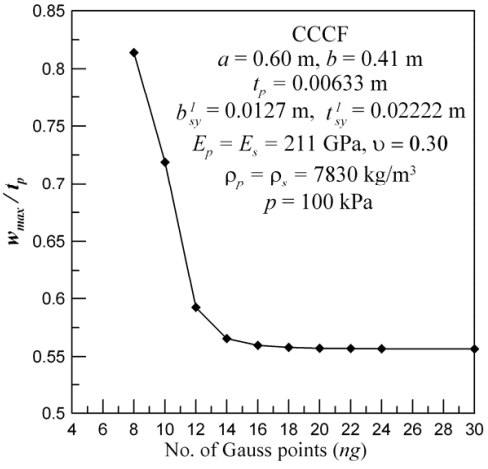

Figure 4. Convergence study for selection of a number of Gauss points.

points dictates the grid density of the computational domain after applying the domain decomposition technique. However, with increase in the stiffener number, the number of subdomains increases and as each subdomain has a grid of $ng \times ng$ reference points, the computations become extensive.

3.1. ***Validation study.*** The formulation and solution methodology used in the present work are validated through comparison with results available in the existing literature. The load-deflection curve obtained from the static analysis incorporating geometric nonlinearity is compared with the results of [Koko and Olson 1992; Rao et al. 1993a; Sheikh and Mukhopadhyay 2000]. A clamped (CCCC) stiffened plate, whose geometry and dimensions (in mm) are provided in Figure 5, left, under uniformly distributed transverse pressure is analyzed and the comparison plots at two different locations on the plate, A and B, are presented in Figure 5, right. Fairly good agreement with the results of other researchers is observed.

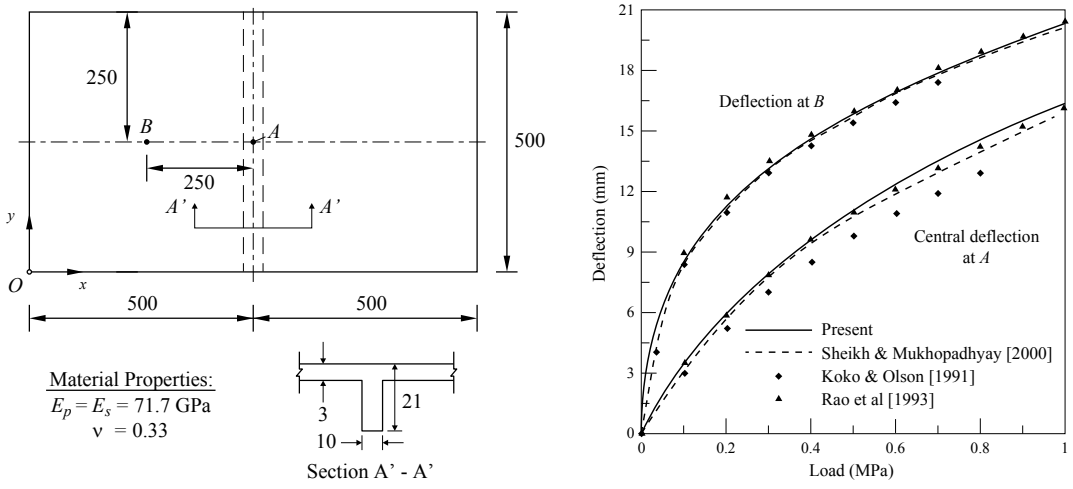

Figure 5. Left: detailed geometry and dimensions of clamped (CCCC) stiffened plate used for validation purpose. Right: comparison of load deflection behavior of clamped stiffened plate at selected points.

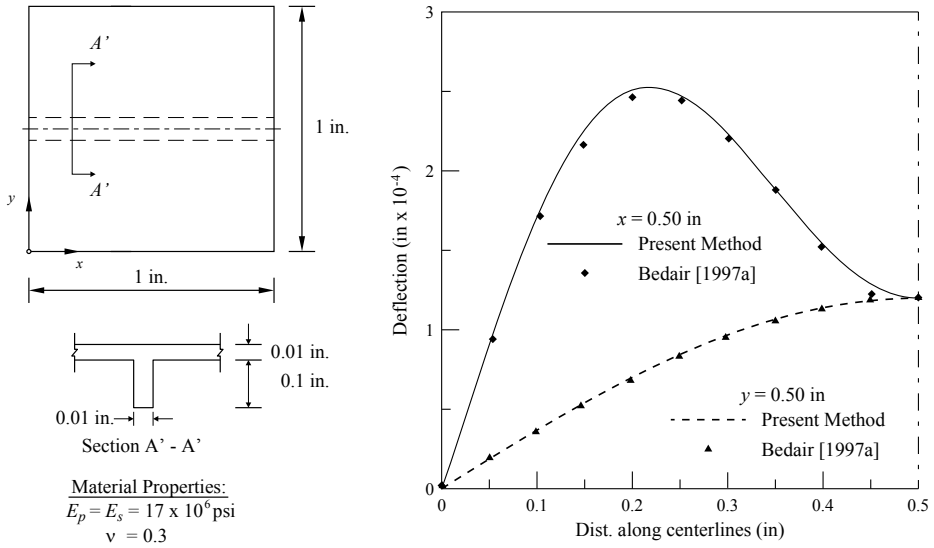

Figure 6. Deflected profile of simply supported square stiffened plate under UDL.

A comparison of the deflected shape of a simply supported (SSSS) square plate with one stiffener under UDL generated through the present method is carried out with results furnished by [Bedair 1997a]. The details of the plate geometry and the material properties are furnished in Figure 6, left, and the results are generated for a uniformly distributed load of 1.0 psi. The comparative plot in Figure 6, right, shows that deflected profiles have identical natures and agreement between the two sets of results is excellent.

The dynamic problem is validated by comparing the linear free vibration frequencies of different modes for a system with reduced complexity. Table 2 shows the free vibration frequency parameters $\omega a^2\sqrt{\rho t_p/D}$ for the first six modes of an unstiffened square plate with various boundary conditions,

Boundary condition	Mode =	1	2	3	4	5	6
CCCC	[Leissa 1973]	24.012	40.029	63.471	76.745	80.704	116.799
	Present	23.939	40.029	63.280	78.031	80.668	118.035
CCSF	[Leissa 1973]	17.621	36.044	52.060	71.182	74.339	106.294
	Present	17.546	36.045	51.851	71.167	75.668	106.324
CSCF	[Leissa 1973]	23.469	35.604	63.135	66.809	77.495	108.985
	Present	23.401	35.606	62.964	67.303	77.496	109.981
CSSF	[Leissa 1973]	16.870	31.128	51.620	64.040	67.637	101.197
	Present	16.806	31.138	51.465	64.563	67.656	102.248
SCSF	[Leissa 1973]	12.679	33.068	41.685	63.005	72.398	90.614
	Present	12.687	33.079	41.715	63.079	73.756	91.115
SSSF	[Leissa 1973]	11.669	27.764	41.193	59.072	61.867	90.278
	Present	11.687	27.772	41.235	59.162	62.391	90.886

Table 2. Comparison of linear dimensionless frequency parameter for an unstiffened plate.

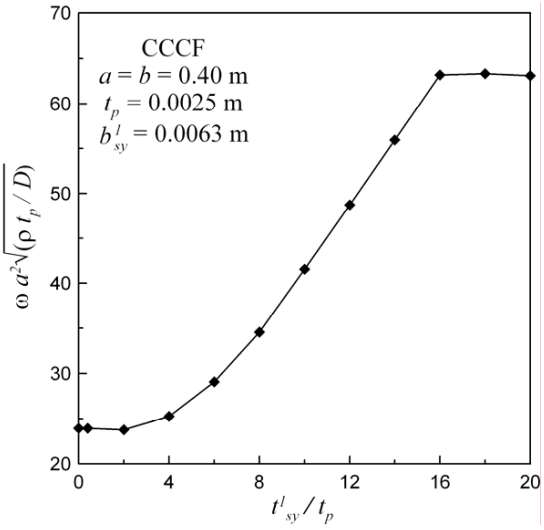

Figure 7. Variation of dimensionless free vibration frequency parameter for the first mode with change in plate-to-stiffener thickness ratio.

comparing them with the results of [Leissa 1973]. For this particular vibration study the stiffener dimensions are taken as zero and good agreement is observed for all the cases. Figure 7 depicts the variation of frequency parameter for the fundamental mode with change in stiffener-to-plate thickness ratio for a square CCCF plate having a single centrally placed eccentric stiffener along the y-direction. The material properties used in this case are as follows: $E_p = E_s = 210\,\text{GPa}$, $\rho_p = \rho_s = 7850\,\text{kg/m}^3$, and $\nu = 0.30$. It is seen that the frequency parameter decreases with decrease in stiffener thickness and as the thickness becomes negligibly small the parameter value converges towards that of an unstiffened plate. The dimensionless frequency parameter of the unstiffened square plate with CCCF boundary is obtained through the present method as 23.939 and, as shown in Table 2, it is in close agreement with the value presented by [Leissa 1973]. The convergence of the frequency parameter towards the value corresponding to an unstiffened plate with decreasing stiffener dimension provides an indirect validation of the present method. Figure 7 also indicates that the dimensionless frequency parameter attains a constant value beyond a particular thickness ratio. At this critical thickness ratio the stiffener divides the plate into two panels of equal width that vibrate with the same natural frequency as the plate. In [Bedair 1997b] a similar trend is observed for simply supported stiffened plates.

3.2. ***Large-amplitude dynamic behavior.*** The present study is undertaken with an objective of investigating the effect of large displacement on the dynamic behavior of stiffened plates and to study the influence of different flexural boundary conditions on the system behavior. The results are presented for a rectangular stiffened plate with $a = 0.60\,\text{m}$, $b = 0.41\,\text{m}$, and $t_p = 0.00633\,\text{m}$, having stiffeners of rectangular cross-section ($0.0127\,\text{m} \times 0.02222\,\text{m}$). The following material properties are used to generate the results: $E_p = E_s = 211\,\text{GPa}$, $\rho_p = \rho_s = 7830\,\text{kg/m}^3$, and $\nu = 0.30$. The nonlinear frequency amplitude relationships of the three different types of stiffened plates (as shown in Figure 2) having typical combinations of boundary conditions are shown graphically as backbone curves in Figures 8–10. These backbone curves have been presented for the first six vibration modes in a nondimensional plane. The

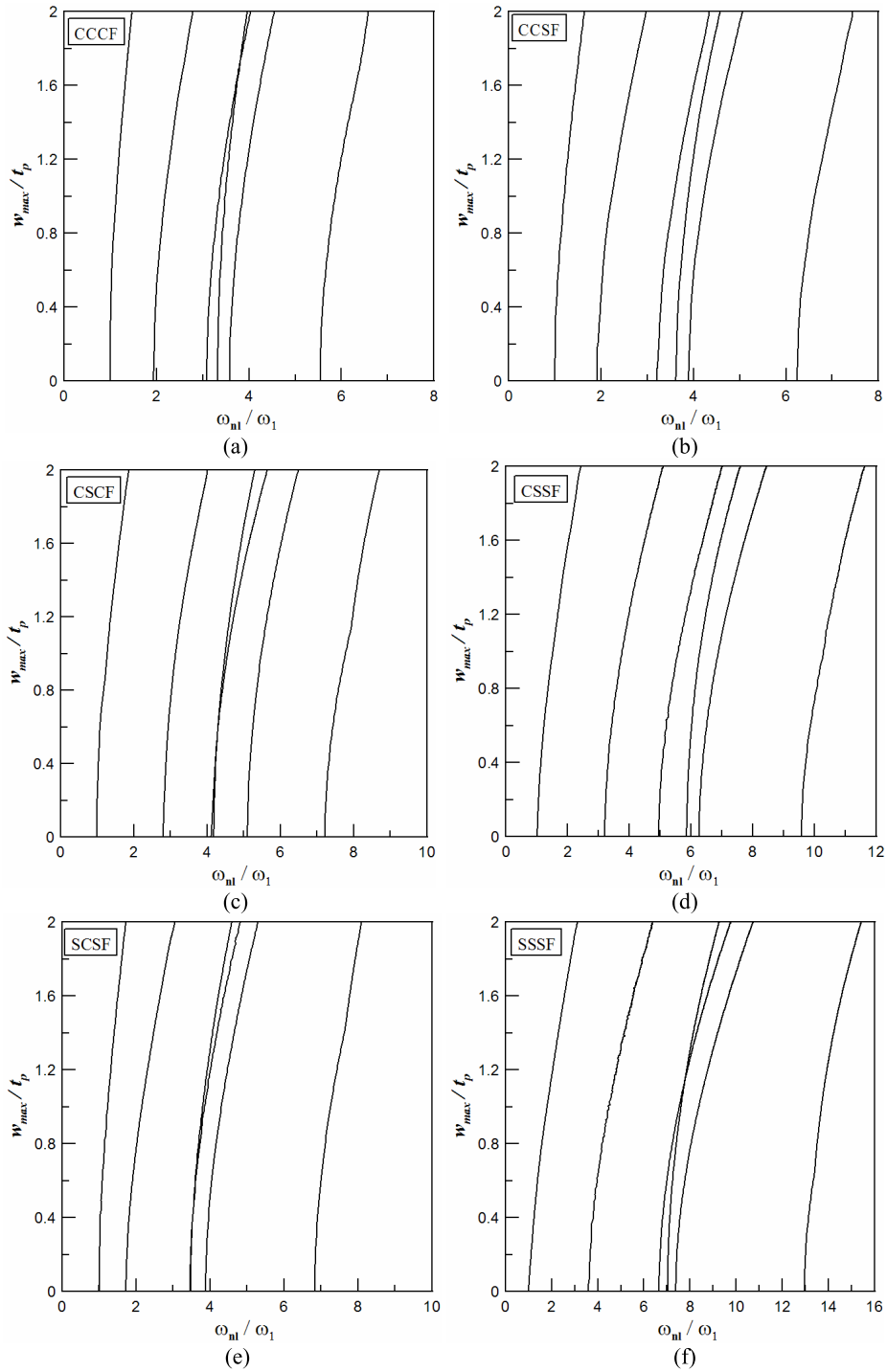

Figure 8. Backbone curves for uniaxially single stiffened rectangular plate under UDL for different boundary conditions with one free edge: (a) CCCF, (b) CCSF, (c) CSCF, (d) CSSF, (e) SCSF, and (f) SSSF.

	Boundary condition					
Type of stiffened plate	CCCF	CCSF	CSCF	CSSF	SCSF	SSSF
Uniaxially single stiffened	148.682	127.015	101.197	72.486	114.094	52.549
Uniaxially double stiffened	154.653	139.136	99.929	84.069	129.423	58.083
Biaxially cross stiffened	199.061	160.732	190.063	144.228	138.142	103.736

Table 3. Fundamental linear frequency (ω_1) in Hz for the three types of stiffened plates with different boundary conditions.

ratio of the maximum transverse deflection to plate thickness is taken as the dimensionless amplitude ($w_{\max}/t_p$) while the nonlinear frequency (ω_{nl}) is normalized by the corresponding fundamental linear frequency (ω_1) to obtain the dimensionless frequency. The results are generated up to a maximum value of dimensionless amplitude ($w_{\max}/t_p$), which is taken as 2.0. The backbone curves for uniaxially single stiffened, uniaxially double stiffened, and biaxially cross stiffened rectangular plates under uniformly distributed transverse load are shown for different boundary conditions, namely CCCF, CCSF, CSCF, CSSF, SCSF, and SSSF, in Figures 8, 9, and 10, respectively. These figures indicate that for a given plate and stiffener geometry the natural frequencies increase as the deflection of the stiffened plate increases for all the cases. In other words, the system exhibits hardening-type nonlinearity. The increase in nonlinear frequency is caused by stiffening of the plate with increasing deflection due to geometric nonlinearity. It is also observed from Figures 8 and 9 that a decrease in rigidity of the boundary conditions, due to introduction of simply supported ends in place of clamped ends, causes the backbone curves for different modes to spread apart in the nondimensional plane. Thus it can be stated that systems with different boundary conditions possess different degrees of nonlinearity.

Mode switching has been observed in a few boundary condition cases for the three types of stiffened plates. Figure 8 shows that for uniaxially single stiffened plates with CCCF, CSCF, SCSF, and SSSF boundary conditions switching occurs between the third (ω_3) and fourth (ω_4) modes. However, a closer inspection reveals that there is also mode switching between the sixth (ω_6) and seventh (ω_7) backbone curves for the cases mentioned above, evident from the slight change in direction of the sixth curve. The absence of the seventh mode gives the sixth curve a broken appearance. In the case of uniaxially double stiffened plates mode switching is absent for all the boundary conditions except SCSF boundaries as shown by Figure 9. From Figure 9e it is clear that first a switch between the fifth (ω_5) and sixth (ω_6) modes takes place and then the fourth (ω_4) and fifth (ω_5) backbone curves intersect each other indicating a further switch. Finally, from the different sets of backbone curves of biaxially cross stiffened plates shown in Figure 10 it is evident that mode switching occurs between fourth (ω_4) and fifth (ω_5) backbone curves for CSCF and SSSF boundaries, whereas no mode switching is observed for the case of CCCF, CCSF, and CSSF conditions. At first glance it seems that this phenomenon is absent in the case of the SCSF boundary condition also. But the discontinuous appearance of the sixth mode indicates that there is indeed a switch between the sixth and seventh backbone curves. The occurrence of mode switching and the modes between which switching occurs depend on parameters such as plate aspect ratio, plate-to-stiffener thickness ratio, stiffener position, stiffener orientation, type of loading, and boundary conditions.

For all the backbone curves, the fundamental linear frequency (ω_1) is used as the normalizing parameter, so its values are provided separately for the three types of stiffened plates with different boundary

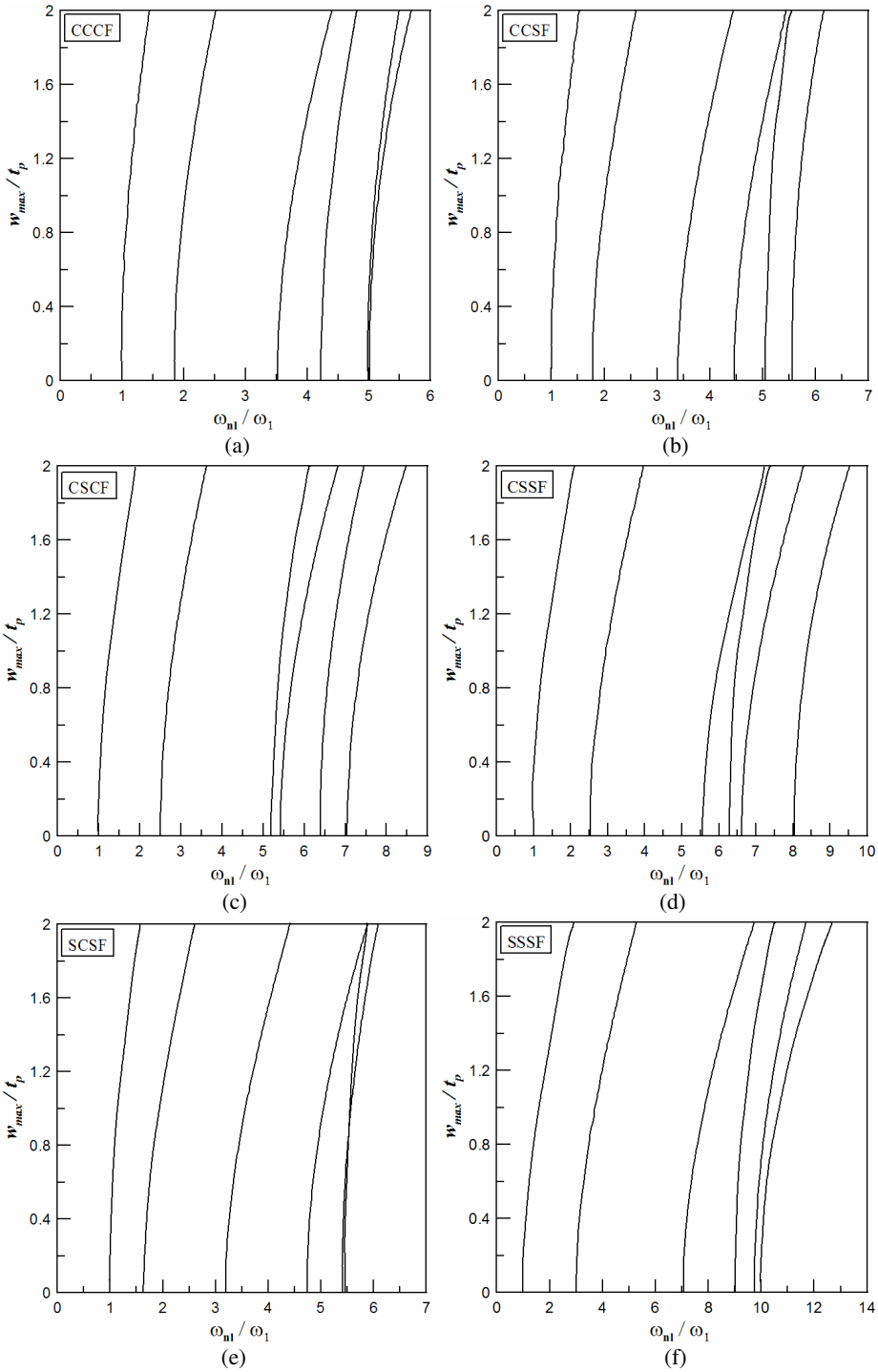

Figure 9. Backbone curves for uniaxially double stiffened rectangular plate under UDL for different boundary conditions with one free edge: (a) CCCF, (b) CCSF, (c) CSCF, (d) CSSF, (e) SCSF, and (f) SSSF.

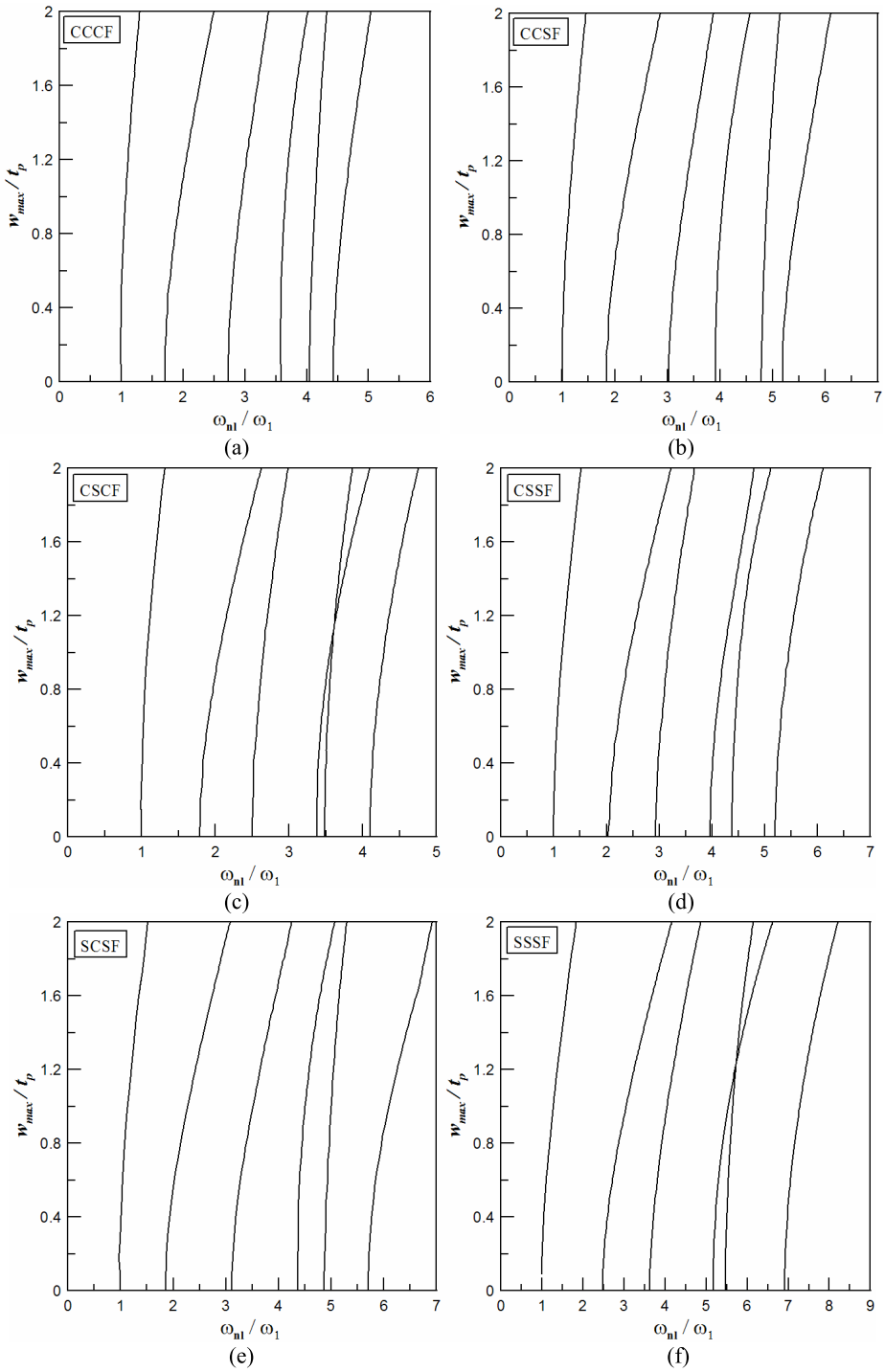

Figure 10. Backbone curves for biaxially cross stiffened rectangular plate under UDL for different boundary conditions with one free edge: (a) CCCF, (b) CCSF, (c) CSCF, (d) CSSF, (e) SCSF, and (f) SSSF.

Type of plate	$w_{\max}/t_p$	ω_{nl}/ω_l Mode = 1	2	3	4	5	6
	0.0	1.000	1.943	3.092	3.329	3.584	5.548
UASS	1.0	1.126	2.176	3.355	3.474	3.867	5.862
	2.0	1.460	2.776	3.958	4.032	4.550	6.581
	0.0	1.000	1.859	3.522	4.230	4.992	5.015
UADS	1.0	1.101	2.020	3.764	4.385	5.098	5.158
	2.0	1.443	2.515	4.396	4.804	5.494	5.691
	0.0	1.000	1.708	2.725	3.588	4.045	4.430
BACS	1.0	1.684	1.954	2.951	3.658	4.141	4.621
	2.0	1.293	2.489	3.379	4.011	4.323	5.037

Table 4. Normalized nonlinear frequency (ω_{nl}/ω_l) for the six modes at $w_{\max}/t_p = 0.0$, 1.0, and 2.0 points on the backbone curve of uniaxially single stiffened (UASS), uniaxially double stiffened (UADS), and biaxially cross stiffened (BACS) plates with the CCCF boundary condition.

conditions in Table 3. It is observed from Table 3 that for a particular type of plate the fundamental linear frequency is highest for the CCCF boundary condition, whereas it is lowest for the SSSF condition. This clearly indicates that clamped-end conditions provide greater rigidity compared to simply supported ends. As a result of the increased stiffness of the system due to end rigidity a higher fundamental frequency is obtained. In the case of uniaxially stiffened plates having a single simply supported end along with the free edge, adjacent clamped ends correspond to a higher fundamental frequency, but for biaxially stiffened plates an opposite trend manifests. Similarly for uniaxially stiffened plates having a single clamped end in addition to the free edge, adjacent simply supported ends correspond to a lower fundamental frequency, but for biaxially stiffened plates the situation is reversed. The table also reveals that the highest stiffness and thus highest fundamental frequency corresponds to cross stiffened plates. Table 4 presents numerical values of normalized nonlinear frequency (ω_{nl}/ω_1) at specific points ($w_{\max}/t_p = 0.0$, 1.0, and 2.0) on the backbone curves for the six modes of three different types of plates having the CCCF boundary condition (shown in Figures 8a, 9a, and 10a).

3.3. ***Mode shape plots.*** To highlight the effect of vibration amplitude on the dynamic behavior in greater detail the mode shape plots for all six vibration modes are presented for the three types of plates in Figures 11–13. For each mode of vibration, two mode shape plots corresponding to linear ($w_{\max}/t_p = 0$) and nonlinear ($w_{\max}/t_p = 2.00$) frequencies are given. In each of these figures, the surface plot and its corresponding contour plot for the vibrating stiffened plate have been presented. The amplitude of vibration is normalized by the absolute difference between the two extremities of the displacement amplitudes. The first six mode shapes for a CCCF uniaxially single stiffened plate under uniform transverse loading are given in Figure 11. Interchange of the linear and nonlinear mode shapes described in Figures 11c and 11d appropriately supports the case of switching between the third and fourth mode. It is also observed from Figure 11f that the linear and nonlinear mode shape plots are totally different, which corroborates that switching occurs between the sixth and seventh modes. The mode shape plots along

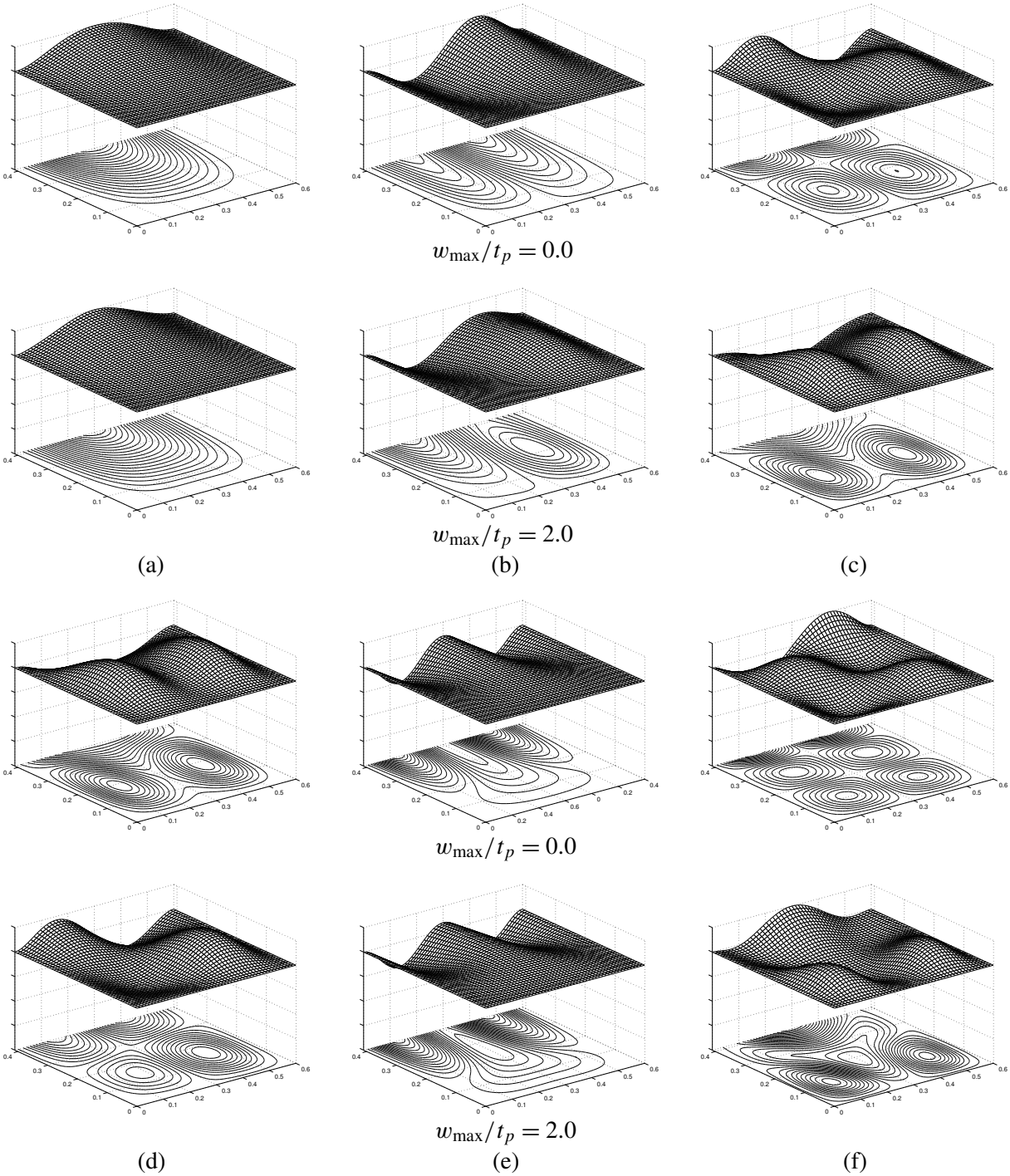

Figure 11. Mode shape plots for uniaxially single stiffened rectangular plate with CCCF boundary condition under UDL: (a) mode 1, (b) mode 2, (c) mode 3, (d) mode 4, (e) mode 5, and (f) mode 6.

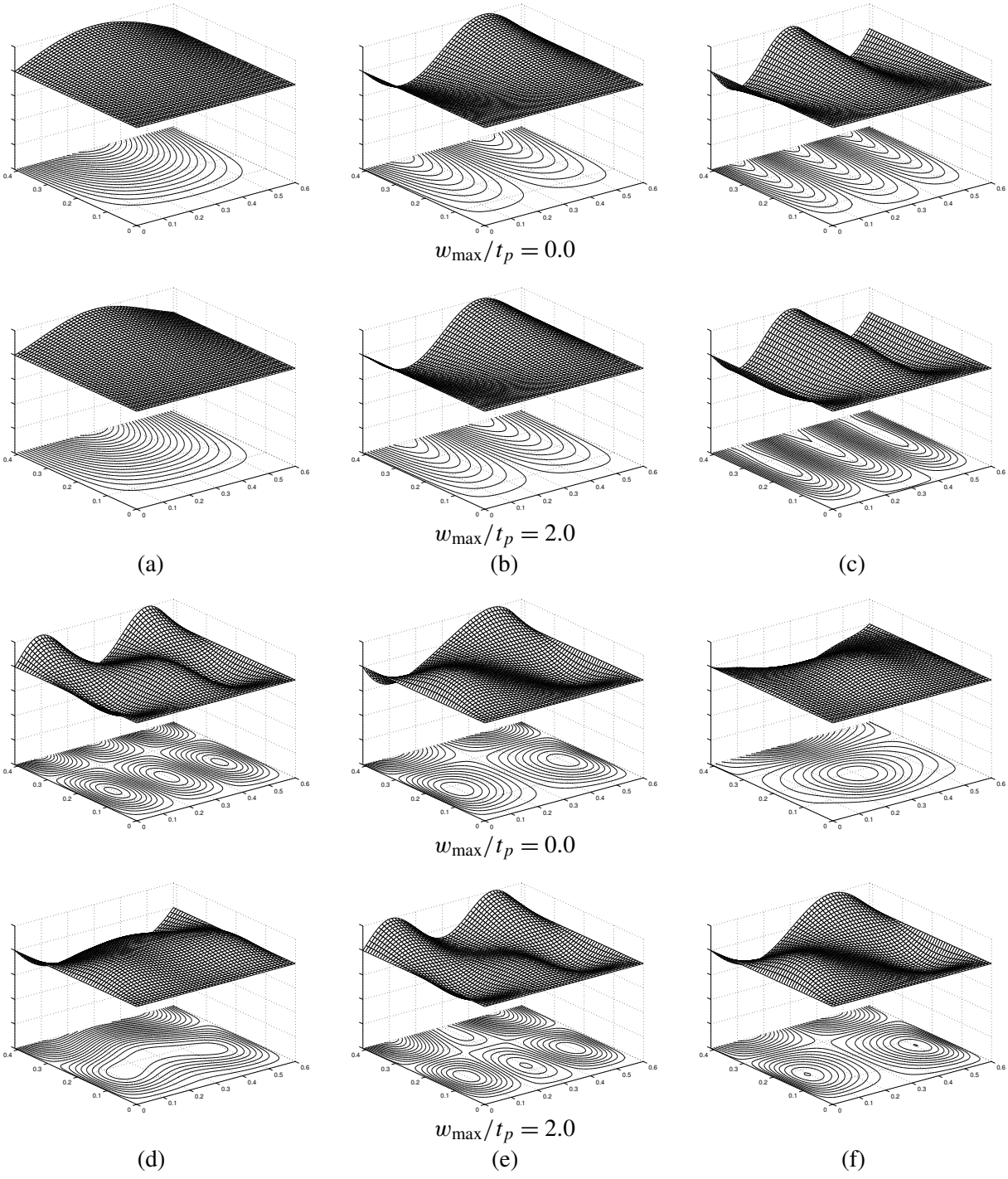

Figure 12. Mode shape plots for uniaxially double stiffened rectangular plate with SCSF boundary condition under UDL: (a) mode 1, (b) mode 2, (c) mode 3, (d) mode 4, (e) mode 5, and (f) mode 6.

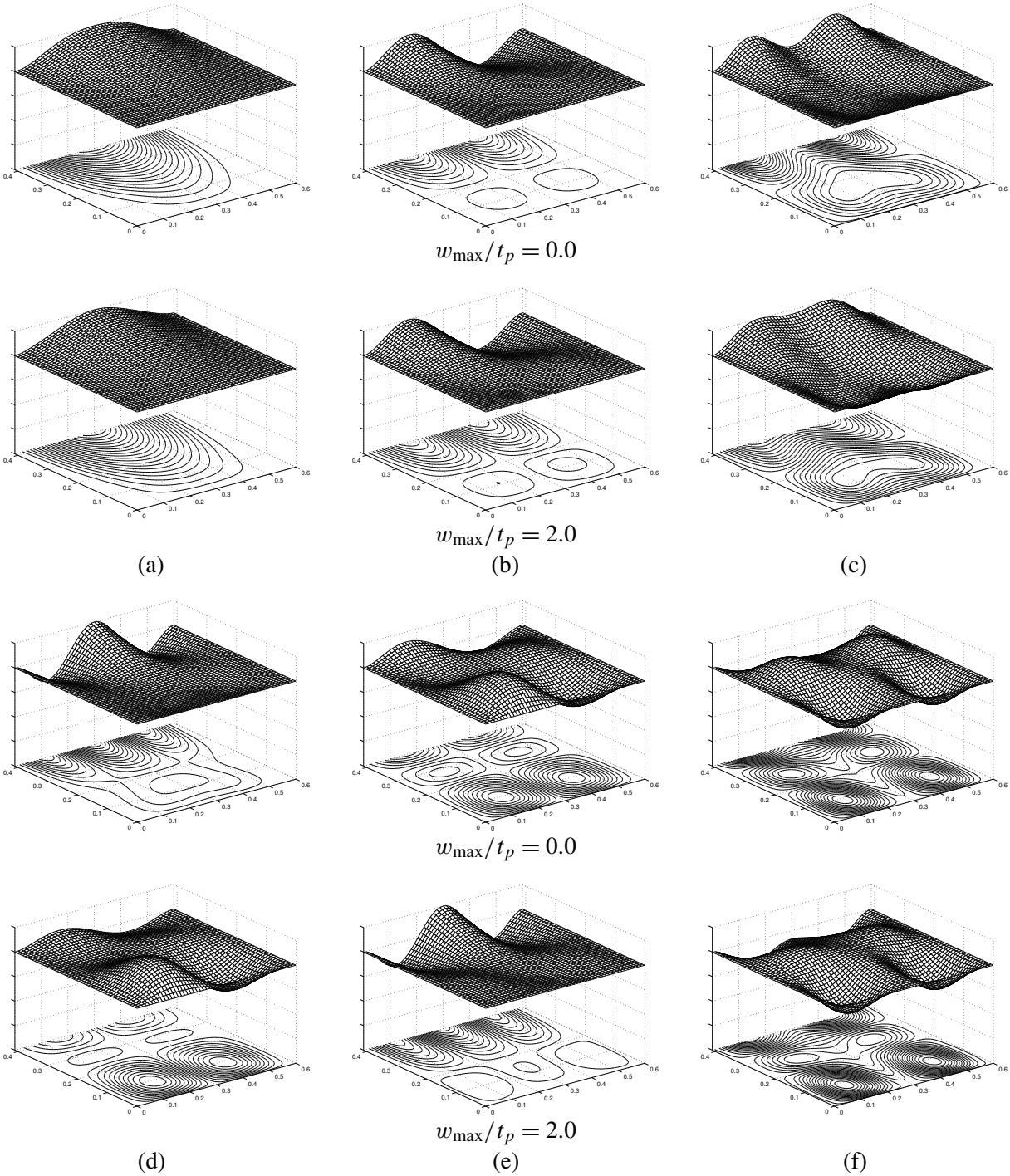

Figure 13. Mode shape plots for biaxially cross stiffened rectangular plate with CSCF boundary condition under UDL: (a) mode 1, (b) mode 2, (c) mode 3, (d) mode 4, (e) mode 5, and (f) mode 6.

with contour plots for all six vibration modes for a uniaxially double stiffened plate are presented in Figure 12, corresponding to SCSF boundary condition (Figure 9e). As expected the mode shape plots in Figure 12d–f support the case of double mode switching. It is clearly seen that the linear mode shape plot in Figure 12d corresponds to the nonlinear mode shape in Figure 12e, the linear mode shape plot in Figure 12e corresponds to the nonlinear mode shape in Figure 12f, and the linear mode shape of Figure 12f is similar to the nonlinear mode shape in Figure 12d. Figure 13 gives the linear and nonlinear mode shape plots for biaxially cross stiffened plates with CSCF boundary conditions. Here interchange of mode shapes between the fourth and fifth modes is observed.

3.4. ***Effect of stiffener position on dynamic behavior.*** The backbone curves of a uniaxially single stiffened plate with CCCF boundary conditions are presented in Figure 14 corresponding to two different stiffener positions, $\eta^1_{\text{stf}} = 1.0$ and $\eta^1_{\text{stf}} = 0.5$, that is, the stiffener is placed parallel to the free edge. In one case the stiffener is positioned at the free edge spanning the length of the plate, whereas for the other the stiffener is at the center of the plate along the x-direction. The figure shows that the general trends of the backbone curves remain identical to those discussed in the preceding section. The effect of shifting the stiffener position on the dynamic behavior of the system is apparent from the changes in the backbone curves of the two cases. For example, switching between the second and third modes of vibration takes place for the central stiffener position as shown in Figure 14b, but the phenomenon is absent for the stiffener placed at the free edge ($\eta^1_{\text{stf}} = 1.0$). The fundamental linear frequencies for the $\eta^1_{\text{stf}} = 1.0$ and $\eta^1_{\text{stf}} = 0.5$ positions of the stiffeners are found as 200.493 and 155.704 Hz, respectively. This indicates that a higher stiffness of the system corresponds to plates with stiffeners at the free edge.

Mode shape plots for the first six vibration modes for a CCCF plate with the stiffener positioned at the free edge are presented in Figure 15. Two mode shape plots corresponding to linear and nonlinear frequencies are provided along with the corresponding contour plots for the vibrating system. Similar to

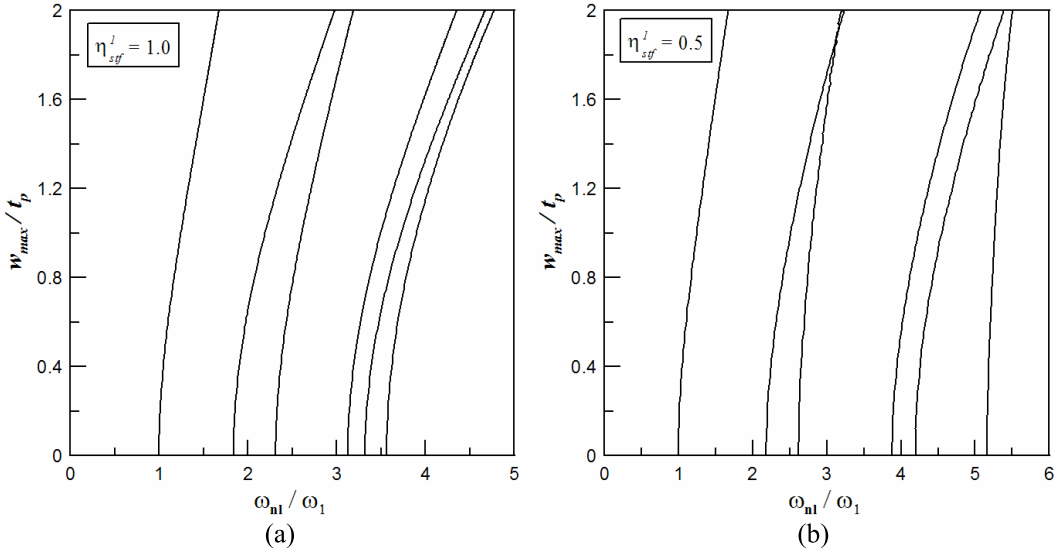

Figure 14. Backbone curves of uniaxially single stiffened rectangular plate with CCCF boundaries for different stiffener positions: (a) $\eta^1_{\text{stf}} = 1.0$ and (b) $\eta^1_{\text{stf}} = 0.5$.

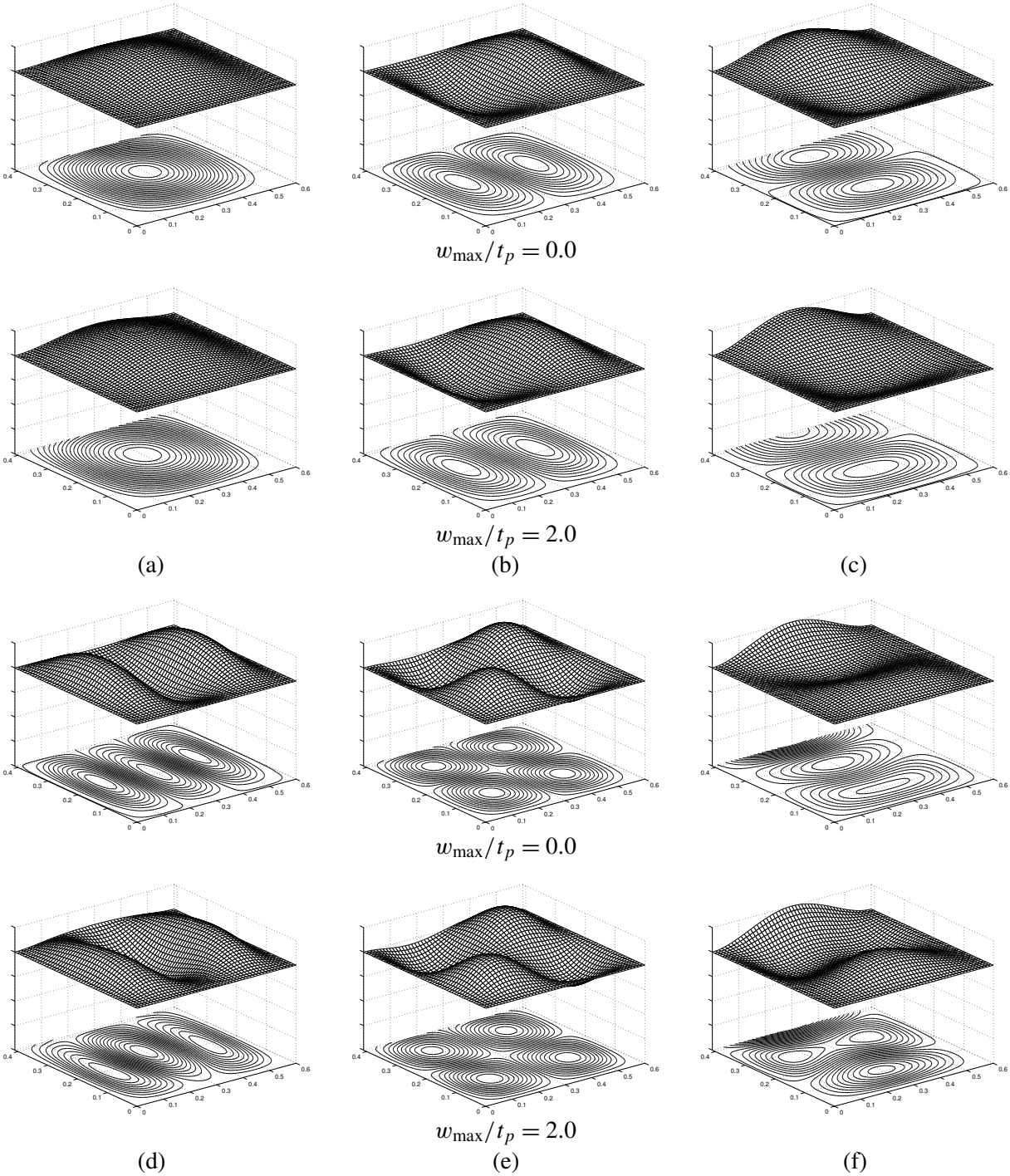

Figure 15. Mode shape plots for uniaxially single stiffened rectangular plate with the stiffener along the free edge, that is, $\eta^1_{\text{stf}} = 1.0$, having CCCF boundary condition: (a) mode 1, (b) mode 2, (c) mode 3, (d) mode 4, (e) mode 5, and (f) mode 6.

Figures 11–13, here also the amplitude of vibration for the surface plots is normalized by the difference between the extremities of the displacement amplitude. It is found that the mode shape plots for linear and nonlinear frequencies are similar in nature. However, minor variations in these mode shape plots are apparent from the contour plots and point to the fact that the amplitude of vibration influences the mode shapes of the system.

4. Conclusion

The present work deals with large-amplitude free-vibration analysis of stiffened plates with various flexural boundary conditions that include a single free edge. The stiffened plates are classified into three categories, by number and orientation of the stiffeners: uniaxially single stiffened, uniaxially double stiffened, and biaxially cross stiffened. A domain decomposition technique is applied to generate the appropriate grid of computation points for the various types of plates. The analysis involves two steps, the first being solution of the static displacement field of the system produced due to a uniformly distributed transverse loading. The second step takes up the free-vibration analysis as an eigenvalue problem on the basis of known static displacement field. The square roots of the computed eigenvalues provide the loaded natural frequencies of the system. The mathematical formulation of the static problem is based on the principle of minimum potential energy, whereas Hamilton's principle has been applied for the dynamic analysis. The results of both static and dynamic analyses are validated with the published results of other researchers and good agreement is observed in almost all the cases. The large-amplitude dynamic behavior has been presented as backbone curves in a dimensionless frequency-amplitude plane. The general trend of the backbone curves indicates hardening-type nonlinearity. Mode switching has been observed for some specific boundary conditions and geometries of the system and the results are adequately backed up by three-dimensional mode shape plots presented along with contour plots in a few specific cases.

Appendix: Details of stiffness matrices and load vector

The form of $[K_b]$ is

$$[K_b] = \begin{bmatrix} k_{11}^b & 0 & 0 \\ 0 & 0 & 0 \\ 0 & 0 & 0 \end{bmatrix},$$

where

$$[k_{11}^b] = D(ab) \sum_{j=1}^{nw} \sum_{i=1}^{nw} \int_0^1 \int_0^1 \left[\left\{ \frac{1}{4}(\phi_{i,\xi\xi})(\phi_{j,\xi\xi}) + \frac{1}{b^4}(\phi_{i,\eta\eta})(\phi_{j,\eta\eta}) + \frac{1}{a^2b^2}(\phi_{i,\xi\xi})(\phi_{j,\eta\eta}) + \frac{1}{a^2b^2}(\phi_{i,\eta\eta})(\phi_{j,\xi\xi}) \right\} - \frac{(1-\nu)}{a^2b^2}\{(\phi_{i,\xi\xi})(\phi_{j,\eta\eta}) + (\phi_{i,\eta\eta})(\phi_{j,\xi\xi}) - 2(\phi_{i,\xi\eta})(\phi_{j,\xi\eta})\} \right] d\xi d\eta.$$

The form of $[K_m]$ is

$$[K_m] = \begin{bmatrix} k_{11}^m & 0 & 0 \\ k_{21}^m & k_{22}^m & k_{23}^m \\ k_{31}^m & k_{32}^m & k_{33}^m \end{bmatrix},$$

where

$$[k_{11}^m] = \frac{E_p t_p}{2(1-\nu^2)}(ab)\sum_{j=1}^{nw}\sum_{i=1}^{nw}\int_0^1\int_0^1\Bigg[\frac{1}{a^4}\Big(\sum_{i=1}^{nw} d_i\phi_{i,\xi}\Big)^2(\phi_{i,\xi})(\phi_{j,\xi}) + \frac{1}{b^4}\Big(\sum_{i=1}^{nw} d_i\phi_{i,\eta}\Big)^2(\phi_{i,\eta})(\phi_{j,\eta})$$
$$+\frac{1}{a^2b^2}\Big(\sum_{i=1}^{nw} d_i\phi_{i,\xi}\Big)^2(\phi_{i,\eta})(\phi_{j,\eta}) + \frac{1}{a^2b^2}\Big(\sum_{i=1}^{nw} d_i\phi_{i,\eta}\Big)^2(\phi_{j,\xi})(\phi_{j,\xi})$$
$$+\frac{2}{a^3}\Big(\sum_{i=nw+1}^{nw+nu} d_i\alpha_{i-nw,\xi}\Big)(\phi_{i,\xi})(\phi_{j,\xi}) + \frac{2}{b^3}\Big(\sum_{i=nw+nu+1}^{nw+nu+nv} d_i\beta_{i-nw-nu,\eta}\Big)(\phi_{i,\eta})(\phi_{j,\eta})$$
$$+\frac{2\nu}{a^2b}\Big(\sum_{i=nw+nu+1}^{nw+nu+nv} d_i\beta_{i-nw-nu,\eta}\Big)(\phi_{i,\xi})(\phi_{j,\xi}) + \frac{2\nu}{ab^2}\Big(\sum_{i=nw+1}^{nw+nu} d_i\alpha_{i-nw,\xi}\Big)(\phi_{i,\eta})(\phi_{j,\eta})$$
$$+\frac{(1-\nu)}{ab^2}\Big\{\Big(\sum_{i=nw+1}^{nw+nu} d_i\alpha_{i-nw,\eta}\Big)(\phi_{i,\xi})(\phi_{j,\eta}) + \Big(\sum_{i=nw+1}^{nw+nu} d_i\alpha_{i-nw,\eta}\Big)(\phi_{i,\eta})(\phi_{j,\xi})\Big\}$$
$$+\frac{(1-\nu)}{a^2b}\Big\{\Big(\sum_{i=nw+nu+1}^{nw+nu+nv} d_i\beta_{i-nw-nu,\xi}\Big)(\phi_{i,\xi})(\phi_{j,\eta}) + \Big(\sum_{i=nw+nu+1}^{nw+nu+nv} d_i\beta_{i-nw-nu,\xi}\Big)(\phi_{i,\eta})(\phi_{j,\xi})\Big\}\Bigg]d\xi d\eta,$$

$$[k_{21}^m] = \frac{E_p t_p}{2(1-\nu^2)}(ab)\sum_{j=nw+1}^{nw+nu}\sum_{i=1}^{nw}\int_0^1\int_0^1\Bigg[\frac{1}{a^3}\Big(\sum_{i=1}^{nw} d_i\phi_{i,\xi}\Big)(\phi_{i,\xi})(\alpha_{j-nw,\xi})$$
$$+\frac{\nu}{ab^2}\Big(\sum_{i=1}^{nw} d_i\phi_{i,\eta}\Big)(\phi_{i,\eta})(\alpha_{j-nw,\xi}) + \frac{(1-\nu)}{ab^2}\Big(\sum_{i=1}^{nw} d_i\phi_{i,\xi}\Big)(\phi_{i,\eta})(\alpha_{j-nw,\eta})\Bigg]d\xi d\eta,$$

$$[k_{22}^m] = \frac{E_p t_p}{2(1-\nu^2)}(ab)\sum_{j=nw+1}^{nw+nu}\sum_{i=nw+1}^{nw+nu}\int_0^1\int_0^1\Bigg[\frac{2}{a^2}(\alpha_{i-nw,\xi})(\alpha_{j-nw,\xi})$$
$$+\frac{(1-\nu)}{b^2}(\alpha_{i-nw,\eta})(\alpha_{j-nw,\eta})\Bigg]d\xi d\eta,$$

$$[k_{23}^m] = \frac{E_p t_p}{2(1-\nu^2)}\sum_{j=nw+1}^{nw+nu}\sum_{i=nw+nu+1}^{nw+nu+nv}\int_0^1\int_0^1\big[2\nu(\beta_{i-nw-nu,\eta})(\alpha_{j-nw,\xi})$$
$$+(1-\nu)(\beta_{i-nw-nu,\xi})(\alpha_{j-nw,\eta})\big]d\xi d\eta,$$

$$[k_{31}^m] = \frac{E_p t_p}{2(1-\nu^2)}(ab)\sum_{j=nw+nu+1}^{nw+nu+nv}\sum_{i=1}^{nw}\int_0^1\int_0^1\Bigg[\frac{1}{b^3}\Big(\sum_{i=1}^{nw} d_i\phi_{i,\eta}\Big)(\phi_{i,\eta})(\beta_{j-nw-nu,\eta})$$
$$+\frac{\nu}{a^2b}\Big(\sum_{i=1}^{nw} d_i\phi_{i,\xi}\Big)(\phi_{i,\xi})(\beta_{j-nw-nu,\eta}) + \frac{(1-\nu)}{a^2b}\Big(\sum_{i=1}^{nw} d_i\phi_{i,\xi}\Big)(\phi_{i,\eta})(\beta_{j-nw-nu,\xi})\Bigg]d\xi d\eta,$$

$$[k_{32}^m] = \frac{E_p t_p}{2(1-\nu^2)}\sum_{j=nw+nu+1}^{nw+nu+nv}\sum_{i=nw+1}^{nw+nu}\int_0^1\int_0^1[2\nu(\alpha_{i-nw,\xi})(\beta_{j-nw-nu,\eta})$$
$$+(1-\nu)(\alpha_{i-nw,\eta})(\beta_{j-nw-nu,\xi})]d\xi d\eta,$$

$$[k_{33}^{m}] = \frac{E_p t_p}{2(1-\nu^2)}(ab) \sum_{j=nw+nu+1}^{nw+nu+nv} \sum_{i=nw+nu+1}^{nw+nu+nv} \int_0^1 \int_0^1 \Bigg[\frac{2}{b^2}(\beta_{i-nw-nu,\eta})(\beta_{j-nw-nu,\eta}) + \frac{(1-\nu)}{a^2}(\beta_{i-nw-nu,\xi})(\beta_{j-nw-nu,\xi}) \Bigg] d\xi\, d\eta.$$

The form of $[K_{sx}]$ is

$$[K_{sx}] = \begin{bmatrix} k_{11}^{sx} & k_{12}^{sx} & 0 \\ k_{21}^{sx} & k_{22}^{sx} & 0 \\ 0 & 0 & k_{33}^{sx} \end{bmatrix},$$

where

$$[k_{11}^{sx}] = \sum_{p=1}^{ns_x} \Bigg[\frac{E_s a}{2} \sum_{j=1}^{nw} \sum_{i=1}^{nw} \int_0^1 \Bigg\{ \frac{2(I_y^p + A_y^p e_x^{p2})}{a^4}(\phi_{i,\xi\xi})(\phi_{j,\xi\xi}) - Q_y^p \frac{2}{a^4}\Big(\sum_{i=1}^{nw} d_i \phi_{i,\xi}\Big)^2 (\phi_{i,\xi\xi})(\phi_{j,\xi}) - Q_y^p \frac{1}{a^4}\Big(\sum_{i=1}^{nw} d_i \phi_{i,\xi}\Big)(\phi_{i,\xi})(\phi_{j,\xi\xi}) + A_y^p \frac{1}{a^4}\Big(\sum_{i=1}^{nw} d_i \phi_{i,\xi}\Big)^2 (\phi_{i,\xi})(\phi_{j,\xi}) + A_y^p \frac{2}{a^3}\Big(\sum_{i=nw+1}^{nw+nu} d_i \alpha_{i-nw,\xi}\Big)^2 (\phi_{i,\xi})(\phi_{j,\xi}) \Bigg\} d\xi \Bigg],$$

$$[k_{12}^{sx}] = \sum_{p=1}^{ns_x} \Bigg[\frac{E_s a}{2} \sum_{j=1}^{nw} \sum_{i=nw+1}^{nw+nu} \int_0^1 \Bigg\{ -Q_y^p \frac{2}{a^3}(\alpha_{i-nw,\xi})(\phi_{j,\xi\xi}) \Bigg\} d\xi \Bigg],$$

$$[k_{21}^{sx}] = \sum_{p=1}^{ns_x} \Bigg[\frac{E_s a}{2} \sum_{j=nw+1}^{nw+nu} \sum_{i=1}^{nw} \int_0^1 \Bigg\{ -Q_y^p \frac{2}{a^3}(\phi_{i,\xi\xi})(\alpha_{j-nw,\xi}) + A_y^p \frac{1}{a^3}\Big(\sum_{i=1}^{nw} d_i \phi_{i,\xi}\Big)(\phi_{i,\xi})(\alpha_{j-nw,\xi}) \Bigg\} d\xi \Bigg],$$

$$[k_{22}^{sx}] = \sum_{p=1}^{ns_x} \Bigg[\frac{E_s a}{2} \sum_{j=nw+1}^{nw+nu} \sum_{i=nw+1}^{nw+nu} \int_0^1 \Bigg\{ A_y^p \frac{2}{a^2}(\alpha_{i-nw,\xi})(\alpha_{j-nw,\xi}) \Bigg\} d\xi \Bigg],$$

$$[k_{33}^{sx}] = \sum_{p=1}^{ns_x} \Bigg[\frac{E_s a}{2} \sum_{j=nw+nu+1}^{nw+nu+nv} \sum_{i=nw+nu+1}^{nw+nu+nv} \int_0^1 \Bigg\{ \frac{2(I_{yz}^p + A_y^p (b\eta_{\mathrm{stf}}^p)^2)}{a^4}(\beta_{i-nw-nu,\xi})(\beta_{j-nw-nu,\xi}) \Bigg\} d\xi \Bigg].$$

The form of $[K_{sy}]$ is

$$[K_{sy}] = \begin{bmatrix} k_{11}^{sy} & 0 & k_{13}^{sy} \\ 0 & k_{22}^{sy} & 0 \\ k_{31}^{sy} & 0 & k_{33}^{sy} \end{bmatrix},$$

where

$$[k_{11}^{sy}] = \sum_{q=1}^{ns_y} \Bigg[\frac{E_s b}{2} \sum_{j=1}^{nw} \sum_{i=1}^{nw} \int_0^1 \Bigg\{ \frac{2(I_x^q + A_x^q e_y^{q2})}{b^4}(\phi_{i,\eta\eta})(\phi_{j,\eta\eta}) - Q_x^q \frac{2}{b^4}\Big(\sum_{i=1}^{nw} d_i \phi_{i,\eta}\Big)^2 (\phi_{i,\eta\eta})(\phi_{j,\eta}) - Q_x^q \frac{1}{b^4}\Big(\sum_{i=1}^{nw} d_i \phi_{i,\eta}\Big)(\phi_{i,\eta})(\phi_{j,\eta\eta}) + A_x^q \frac{1}{b^4}\Big(\sum_{i=1}^{nw} d_i \phi_{i,\eta}\Big)^2 (\phi_{i,\eta})(\phi_{j,\eta}) + A_x^q \frac{2}{b^3}\Big(\sum_{i=nw+1}^{nw+nu} d_i \beta_{i-nw,\eta}\Big)^2 (\phi_{i,\eta})(\phi_{j,\eta}) \Bigg\} d\eta \Bigg],$$

$$[k_{22}^{sy}] = \sum_{q=1}^{ns_y}\left[\frac{E_s b}{2}\sum_{j=nw+1}^{nw+nu}\sum_{i=nw+1}^{nw+nu}\int_0^1\left\{\frac{2(I_{xz}^q + A_x^q(a\xi_{\mathrm{stf}}^q)^2)}{b^4}(\alpha_{i-nw},_{\eta\eta})(\alpha_{j-nw},_{\eta\eta})\right\}d\eta\right],$$

$$[k_{33}^{sy}] = \sum_{q=1}^{ns_y}\left[\frac{E_s b}{2}\sum_{j=nw+nu+1}^{nw+nu+nv}\sum_{i=nw+nu+1}^{nw+nu+nv}\int_0^1\left\{A_x^q\frac{2}{b^2}(\beta_{i-nw-nu},_{\eta})(\beta_{j-nw-nu},_{\eta})\right\}d\eta\right],$$

$$[k_{31}^{sy}] = \sum_{q=1}^{ns_y}\left[\frac{E_s b}{2}\sum_{j=nw+nu+1}^{nw+nu+nv}\sum_{i=1}^{nw}\int_0^1\left\{-Q_x^q\frac{2}{b^3}(\phi_i,_{\eta\eta})(\beta_{j-nw-nu},_{\eta}) + A_x^q\frac{1}{b^3}\Big(\sum_{i=1}^{nw}d_i\phi_i,_{\eta}\Big)(\phi_i,_{\eta})(\beta_{j-nw-nu},_{\eta})\right\}d\eta\right],$$

$$[k_{13}^{sy}] = \sum_{q=1}^{ns_y}\left[\frac{E_s b}{2}\sum_{j=1}^{nw}\sum_{i=nw+nu+1}^{nw+nu+nv}\int_0^1\left\{-Q_x^q\frac{2}{b^3}(\beta_{i-nw-nu},_{\eta})(\phi_j,_{\eta\eta})\right\}d\eta\right].$$

The load vector $\{f\}$ is of the form $\{f\} = \begin{Bmatrix} f_{11} & f_{12} & f_{13}\end{Bmatrix}^T$, where $\{f_{11}\} = p(ab)\sum_{j=1}^{nw}\int_0^1\int_0^1\phi_j\,d\xi\,d\eta$, $\{f_{12}\} = \{f_{13}\} = 0$. In the present analysis, results are individually generated for uniformly distributed load $\left(\{f_{11}\} = p(ab)\sum_{j=1}^{nw}\int_0^1\int_0^1\phi_j\,d\xi\,d\eta\right)$.

List of symbols

a, b	length and width of the plate
b_{sx}^p, b_{sy}^p	width of p-th stiffener along the x- and y-directions
$\{d\}$	vector of unknown coefficients
e_x^p, e_y^p	eccentricity of p-th stiffener along the x- direction and y-directions
E_p	elastic modulus of the plate material
E_s	elastic modulus of the stiffener material
$\{f\}$	load vector
$[K]$	stiffness matrix
$[K_b]$	stiffness matrix due to bending
$[K_m]$	stiffness matrix due to stretching
$[K_{sx}]^p$, $[K_{sy}]^p$	stiffness matrices of the p-th stiffener along the x- and y-directions
$[M]$	mass matrix
$[M_p]$	mass matrix for plate
$[M_{sx}]$, $[M_{sy}]$	mass matrix for the x and y-direction stiffeners
ns_x, ns_y	number of stiffeners in the x and y-directions
nw, nu, nv	number of constituent functions for w, u, and v
p	uniformly distributed transverse load
P	concentrated transverse load
t_p	thickness of the plate
t_{sx}^p, t_{sy}^p	thickness of p-th stiffener along the x- and y-directions
T	total kinetic energy of the system

T_p	kinetic energy of the plate
T_s	total kinetic energy of the stiffeners
T_{sx}^p, T_{sy}^p	kinetic energy of the p-th stiffener along the x- and y-directions
u, v, w	displacement along the x, y, and z-directions
U	total strain energy of the system
U_b	strain energy due to bending of the plate
U_m	strain energy due to stretching of the plate
U_p	strain energy of the plate
U_s	strain energy of the stiffeners
U_{sx}^p, U_{sy}^p	strain energy of the p-th stiffener along the x- and y-directions
V	work potential
x_{stf}^p, y_{stf}^p	position of p-th stiffener along the x- and y-directions
α_i	set of functions defining approximate displacement field u
β_i	set of functions defining approximate displacement field v
δ	variational operator
ε	predefined value of error limit for the iteration scheme
ϕ_i	set of functions defining approximate displacement field w
η	normalized coordinates in the y-direction
λ	relaxation parameter
ρ_p, ρ_s	density of the plate and stiffener material
τ	time coordinate
ν	Poisson's ratio
ω	natural frequency of the system
ω_1	first linear natural frequency
ω_{nl}	nonlinear frequency
ξ	normalized coordinates in the x-direction

References

[Aksu 1982] G. Aksu, "Free vibration analysis of stiffened plates by including the effect of inplane inertia", *J. Appl. Mech.* (*ASME*) **49**:1 (1982), 206–212.

[Aksu and Ali 1976] G. Aksu and R. Ali, "Free vibration analysis of stiffened plates using finite difference method", *J. Sound Vib.* **48**:1 (1976), 15–25.

[Bapu Rao et al. 1978] M. N. Bapu Rao, P. Guruswamy, M. V. Rao, and S. Pavithran, "Studies on vibration of some rib-stiffened cantilever plates", *J. Sound Vib.* **57**:3 (apr 1978), 389–402.

[Barrette et al. 2000] M. Barrette, A. Berry, and O. Beslin, "Vibration of stiffened plates using hierarchical trigonometric functions", *J. Sound Vib.* **235**:5 (2000), 727–747.

[Bedair 1997a] O. K. Bedair, "Analysis of stiffened plates under lateral loading using sequential quadratic programming (SQP)", *Comput. Struct.* **62**:1 (1997), 63–80.

[Bedair 1997b] O. K. Bedair, "Fundamental frequency determination of stiffened plates using sequential quadratic programming", *J. Sound Vib.* **199**:1 (1997), 87–106.

[Bedair and Troitsky 1997] O. K. Bedair and M. S. Troitsky, "A study of the fundamental frequency characteristics of eccentrically and concentrically simply supported stiffened plates", *Int. J. Mech. Sci.* **39**:11 (1997), 1257–1272.

[Bikri et al. 2003] K. E. Bikri, R. Benamar, and M. Bennouna, "Geometrically non-linear free vibrations of clamped simply supported rectangular plates. Part I: the effects of large vibration amplitudes on the fundamental mode shape", *Comput. Struct.* **81**:20 (2003), 2029–2043.

[Blevins 1981] R. D. Blevins, *Formulas for the Natural Frequency and Mode Shape*, Van Nostrand, New York, 1981.

[Chen et al. 1994] C. J. Chen, W. Liu, and S. M. Chern, "Vibration analysis of stiffened plates", *Comput. Struct.* **50**:4 (1994), 471–480.

[Cook et al. 1989] R. D. Cook, D. S. Malkus, and M. E. Plesha, *Concepts and Applications of Finite Element Analysis*, Wiley, 1989.

[Crandall 1956] S. H. Crandall, *Engineering Analysis: A Survey of Numerical Procedures*, McGrawMHill, 1956.

[Das et al. 2009] D. Das, P. Sahoo, and K. Saha, "Nonlinear vibration analysis of clamped skew plates by a variational method", *J. Vib. Control* **15**:7 (2009), 985–1017.

[Deb Nath et al. 2010] S. K. Deb Nath, S. R. Ahmed, and S.-G. Kim, "Analytical solution of a stiffened orthotropic plate using alternative displacement potential approach", *J. Aerospace Eng.* **224**:1 (2010), 89–99.

[Dozio and Ricciardi 2009] L. Dozio and M. Ricciardi, "Free vibration analysis of ribbed plates by a combined analytical-numerical method", *J. Sound Vib.* **319**:1-2 (2009), 681–697.

[Harik and Guo 1993] I. E. Harik and M. Guo, "Finite element analysis of eccentrically stiffened plates in free vibration", *Comput. Struct.* **49**:6 (1993), 1007–1015.

[Irie et al. 1982] T. Irie, G. Yamada, and H. Ida, "Free vibration of a stiffened trapezoidal cantilever plate", *J. Acoust. Soc. Am.* **72** (1982), 1508–1513.

[Koko and Olson 1992] T. S. Koko and M. D. Olson, "Vibration analysis of stiffened plates by super elements", *J. Sound Vib.* **158**:1 (1992), 149–167.

[Leissa 1973] A. W. Leissa, "The free vibration of rectangular plates", *J. Sound Vib.* **31**:3 (1973), 257–293.

[Mukherjee and Mukhopadhyay 1986] A. Mukherjee and M. Mukhopadhyay, "A review of dynamic behavior of stiffened plates", *Shock Vib. Digest* **18**:6 (1986), 3–8.

[Mukherjee and Mukhopadhyay 1988] A. Mukherjee and M. Mukhopadhyay, "Finite element free vibration of eccentrically stiffened plates", *Comput. Struct.* **30**:6 (1988), 1303–1317.

[Peng et al. 2006] L. X. Peng, K. M. Liew, and S. Kitipornchai, "Buckling and free vibration analyses of stiffened plates using the FSDT mesh-free method", *J. Sound Vib.* **289**:3 (2006), 421–449.

[Prathap and Varadan 1978] G. Prathap and T. K. Varadan, "Large amplitude flexural vibration of stiffened plates", *J. Sound Vib.* **57**:4 (1978), 583–593.

[Rao et al. 1993a] D. V. Rao, A. H. Sheikh, and M. Mukhopadhyay, "A finite element large displacement analysis of stiffened plates", *Comput. Struct.* **47**:6 (1993), 987–993.

[Rao et al. 1993b] S. R. Rao, A. H. Sheikh, and M. Mukhopadhyay, "Large-amplitude finite element flexural vibration of plates/stiffened plates", *J. Acoust. Soc. Am.* **93** (1993), 3250–3257.

[Reddy 2002] J. N. Reddy, *Energy principles and variational methods in applied mechanics*, John Wiley & Sons Inc, 2002.

[Rossi et al. 1998] R. E. Rossi, D. V. Bambill, and P. A. A. Laura, "Vibrations of a rectangular orthotropic plate with a free edge: A comparison of analytical and numerical results", *Ocean Eng.* **25**:7 (1998), 521–527.

[Saha et al. 2004] K. N. Saha, D. Misra, G. Pohit, and S. Ghosal, "Large amplitude free vibration study of square plates under different boundary conditions through a static analysis", *J. Vib. Control* **10**:7 (2004), 1009–1028.

[Sapountzakis and Mokos 2008] E. J. Sapountzakis and V. G. Mokos, "An improved model for the dynamic analysis of plates stiffened by parallel beams", *Eng. Struct.* **30**:6 (2008), 1720–1733.

[Sheikh and Mukhopadhyay 2000] A. H. Sheikh and M. Mukhopadhyay, "Geometric nonlinear analysis of stiffened plates by the spline finite strip method", *Comput. Struct.* **76**:6 (2000), 765–785.

[Shuyu 2001] L. Shuyu, "Study on the flexural vibration of rectangular thin plates with free boundary conditions", *J. Sound Vib.* **239**:5 (2001), 1063–1071.

[Varadan and Pandalai 1979] T. K. Varadan and K. A. V. Pandalai, "Large amplitude flexural vibration of eccentrically stiffened plates", *J. Sound Vib.* **67**:3 (1979), 329–340.

[Vörös 2009] G. M. Vörös, "Buckling and free vibration analysis of stiffened panels", *Thin-Walled Struct.* **47**:4 (2009), 382–390.

[Wang and Xu 2010] X. Wang and S. Xu, "Free vibration analysis of beams and rectangular plates with free edges by the discrete singular convolution", *J. Sound Vib.* **329**:10 (2010), 1780–1792.

[Xu et al. 2010] H. Xu, J. Du, and W. L. Li, "Vibrations of rectangular plates reinforced by any number of beams of arbitrary lengths and placement angles", *J. Sound Vib.* **329**:18 (2010), 3759–3779.

[Zeng and Bert 2001] H. Zeng and C. W. Bert, "A differential quadrature analysis of vibration for rectangular stiffened plates", *J. Sound Vib.* **241**:2 (2001), 247–252.

Received 23 Aug 2010. Revised 12 Jan 2011. Accepted 13 Jan 2011.

ANIRBAN MITRA: samik893@gmail.com
Department of Mechanical Engineering, Jadavpur University, Kolkata 700 032, India

PRASANTA SAHOO: psjume@gmail.com
Department of Mechanical Engineering, Jadavpur University, Kolkata 700 032, India

KASHINATH SAHA: kashinathsaha@gmail.com
Department of Mechanical Engineering, Jadavpur University, Kolkata 700 032, India
http://www.jaduniv.edu.in/profile.php?uid=490

JOURNAL OF MECHANICS OF MATERIALS AND STRUCTURES

jomms.org

Founded by Charles R. Steele and Marie-Louise Steele

See http://jomms.org for submission guidelines.

JoMMS (ISSN 1559-3959) is published in 10 issues a year. The subscription price for 2011 is US $520/year for the electronic version, and $690/year (+$60 shipping outside the US) for print and electronic. Subscriptions, requests for back issues, and changes of address should be sent to Mathematical Sciences Publishers, Department of Mathematics, University of California, Berkeley, CA 94720–3840.

JoMMS peer-review and production is managed by EditFLOW™ from Mathematical Sciences Publishers.

PUBLISHED BY
mathematical sciences publishers
http://msp.org/

A NON-PROFIT CORPORATION

Typeset in LaTeX

Journal of Mechanics of Materials and Structures

Volume 6, No. 6 July–August 2011

1559-3959(2011)6:6;1-A